SECTION B

CHAPTER 3

RESULTS AND DISCUSSION*,[1]

SPECTROSCOPIC , MICROSCOPIC AND ELECTROCHEMICAL PROPERTIES OF IRON-PHTHALOCYANINE SINGLE-WALLED CARBON NANOTUBE BASED ELECTRODES

*Chapters 3 – 6 comprise the results and discussion.

[1]Five publications resulted from work presented in these chapters and they are not referenced further in this thesis.

3.1 SAM formation strategies

The stepwise self-assembly strategy employed in the preparation of the main electrodes is schematically represented in the Scheme 3.1 following the established procedure. For simplicity, the gold electrodes modified with the cysteamine is represented as Au-Cys, the Au-Cys integrated with single-walled carbon nanotubes is represented as Au-Cys-SWCNT, while the Au-Cys-SWCNT integrated with the FeOHETPc as the Au-Cys-SWCNT-FeOHETPc.

Upon acid treatment, single-walled carbon nanotubes bear most of the carboxylic acid groups which are found at the end of these tubes, the edge-plane and or defect sites of the tubes. Few appearance of the functional groups at the defect sites of the walls are also possible as depicted in scheme 3.1. The fabrication of Au-Cys-SWCNT-FeTAPc followed a similar protocol. Also, the Au-FeOHETPc was prepared as reported by Ozoemena *et al.* [1], while the Au-FeTAPc electrode was fabricated using the method described by Somashekarappa *et al.* [2].

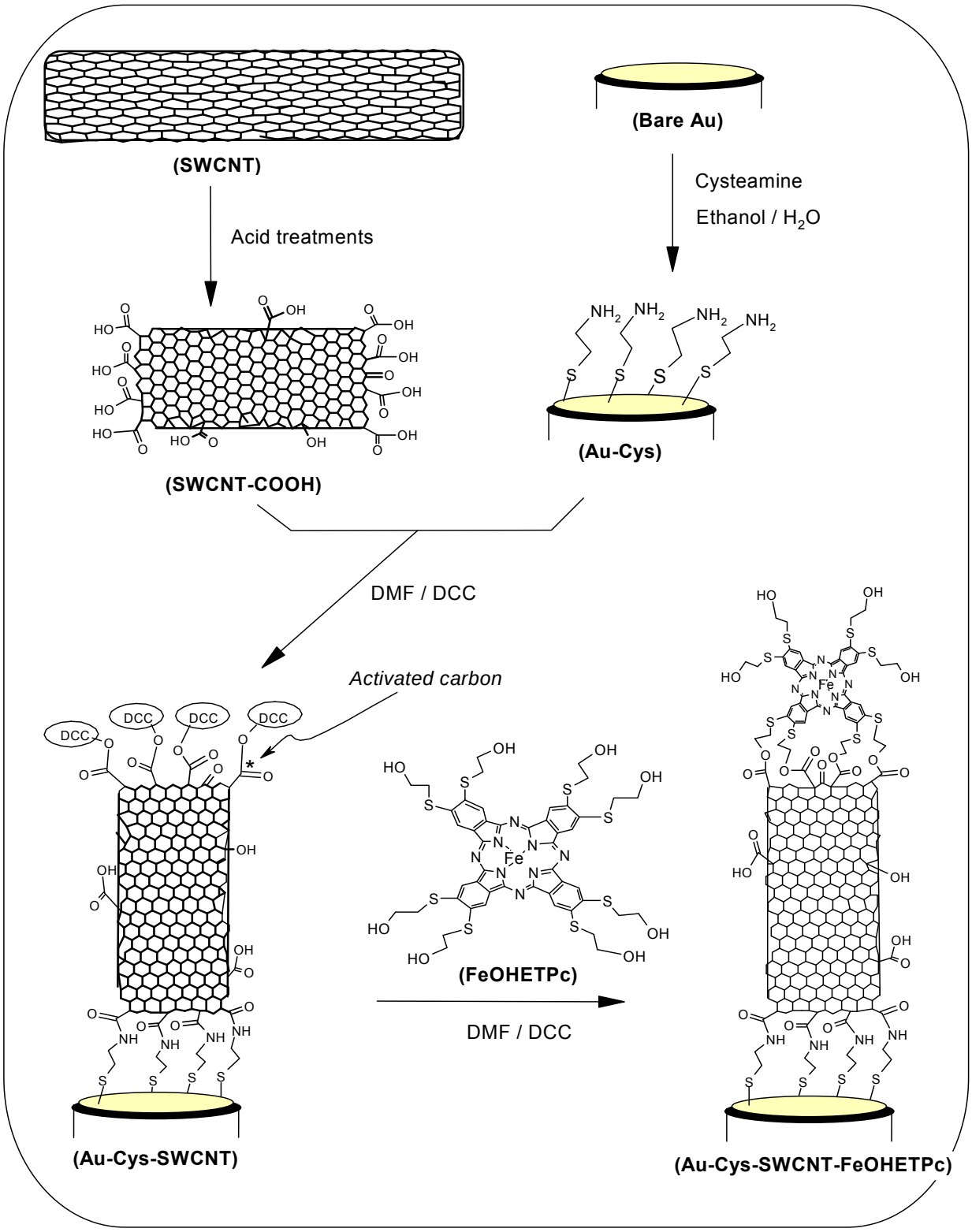

Scheme 3.1: Schematic representation of the self-assembly processes of the SWCNT and SWCNT-FeOHETPc on gold electrode.

3.2 Atomic force microscopy characterization

AFM studies were conducted to give an insight to the surface morphologies of the formed SAMs and figure 3.1 exemplifies the 3-D AFM images of the Au-Cys (a), Au-Cy-SWCNT (b) and Au-Cys-SWCNT-FeOHETPc (c), indicating that the SAMs assume perpedincular orientations on the gold surfaces.

The needle-like protrusions are in agreement with several literature reports for SWCNT-based SAMs [3-5]. If we realise that as many as eight carboxyl groups might be present at each end of a ~1.3 nm-diameter SWCNT [4], it is reasonable therefore to assume that about eight amide bonds could be generated between each SWCNT and the modified gold surface, hence explaining the preferred vertical alignment of the SWCNT onto the gold surface.

The strong van der Waal's attractive forces existing between carbon nanotubes should make SWCNTs assemble as bundles and not as individual. This is even more possible given that Au-Cys SAM (Figure 3.1(a)) also exist as bundles because of this attractive force. According to literature [3], SWCNTs prefer to assemble on gold surfaces as bundles of around 5 – 20 tubes. It is apparent from the images shown in figure 3.1(a) that the aligned SWCNTs did not assemble on the gold surface as individual tubes but as bundles.

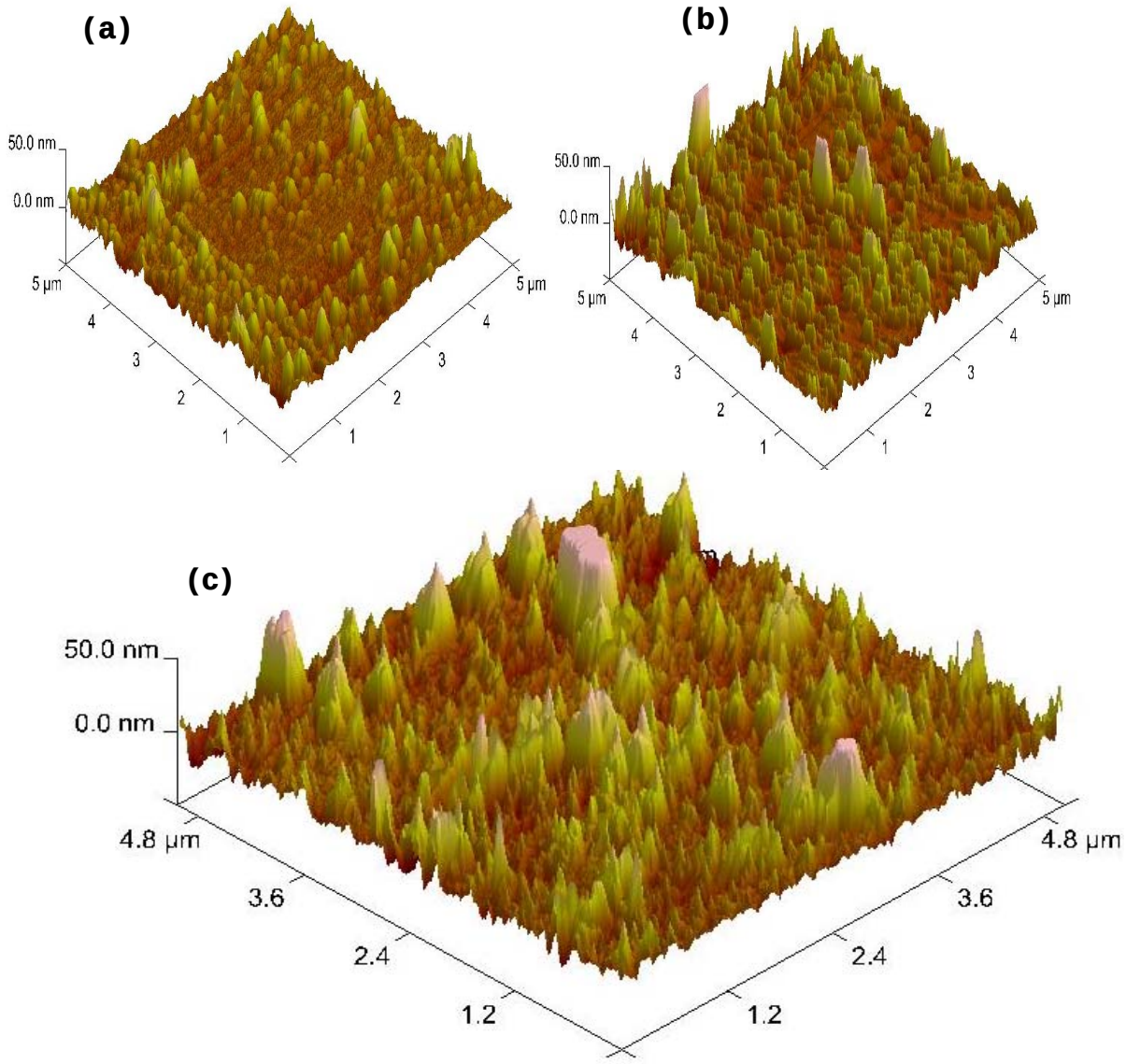

Figure 3.1: Typical AFM images of aligned (a) Cys, (b) Cys-SWCNT and (c) Cys-SWCNT-FeOHETPc modified gold surfaces.

Although, the 'cut' SWCNTs were not fractionalized before being immobilized onto the gold electrodes, it is interesting to observe that the heights of the vertically aligned SWCNT bundles still lie in the ~ 30

– 50 nm range, as observed in previous reports [3-5]. The AFM images obtained on subsequent coupling of the FeOHETPc onto the Au-Cys-SWCNT surface (reaction time 25 hr) (Figure 3.1(b)) expectedly shows similar bundled shapes of the Au-Cys-SWCNT. However, unlike in figure 3.1(b), the FeOHETPc showed more defined needle-like protrusions, with slight increase (*ca*. 2 nm) in the average bundle lengths, suggesting that the FeOHETPc species are linked to the ends of the SWCNTs (few binding on the defect sites of the sidewalls of the SWCNTs may not be completely ruled out). Li *et al.* [6] predicted from computer modelling that MPc containing eight peripheral substituents, R, (R = $O(CH_2)_4CH_3$) has a diameter of 21 Å. In this work, where R = $S(CH_2)_2OH$, it means that the diameter of the FeOHETPc (if modelled as a circle) with standing (vertical) orientation as depicted in Scheme 1 may be assumed to be about 20 Å (i.e., ~ 2 nm). This value certainly explains the insignificant change in the length of Au-Cys-SWCNT-FeOHETPc compared to that of the Au-Cys-SWCNT shown by the AFM experiments.

3.3 XPS characterization

Having confirmed the formation of the SAMs on gold surfaces by AFM experiments, XPS was carried out to give some insights into the elemental compositional details of the self-assembled nanostructures. Figure 3.2 shows the survey X-ray photoelectron spectra for the full (Figure 3.2(a)) and the expanded portions of regions of most interests; sulphur (2p) (Figure3.2(b)), nitrogen (1s) (Figure 3.2(c) and carbon (1s) (Figure 3.2(d)) for the bare Au (i), Au-Cys (ii), Au-Cys-SWCNT (iii), and Au-Cys-SWCNT-FeOHETPc (iv) electrodes.

It is well recognized in XPS [6,7] that oxygen and carbon are almost always present on gold surfaces due to contaminations, the most reliable indicators for the formation of the SAMs studied here are the peaks due to sulphur and nitrogen, however, the carbon peaks give some insights into the presence of the CO and COOH. Calibrating the binding energies using the normal carbon 1s peak of adventitious carbon at 284.5 eV, the sulphur (2p) peak for both Au-Cys and Au-Cys-SWCNT appeared at 161.5 eV, assigned to the normal Au-S bond [6-12], while that for the Au-Cys-SWCNT-FeOHETPc was observed at 162.5 eV.

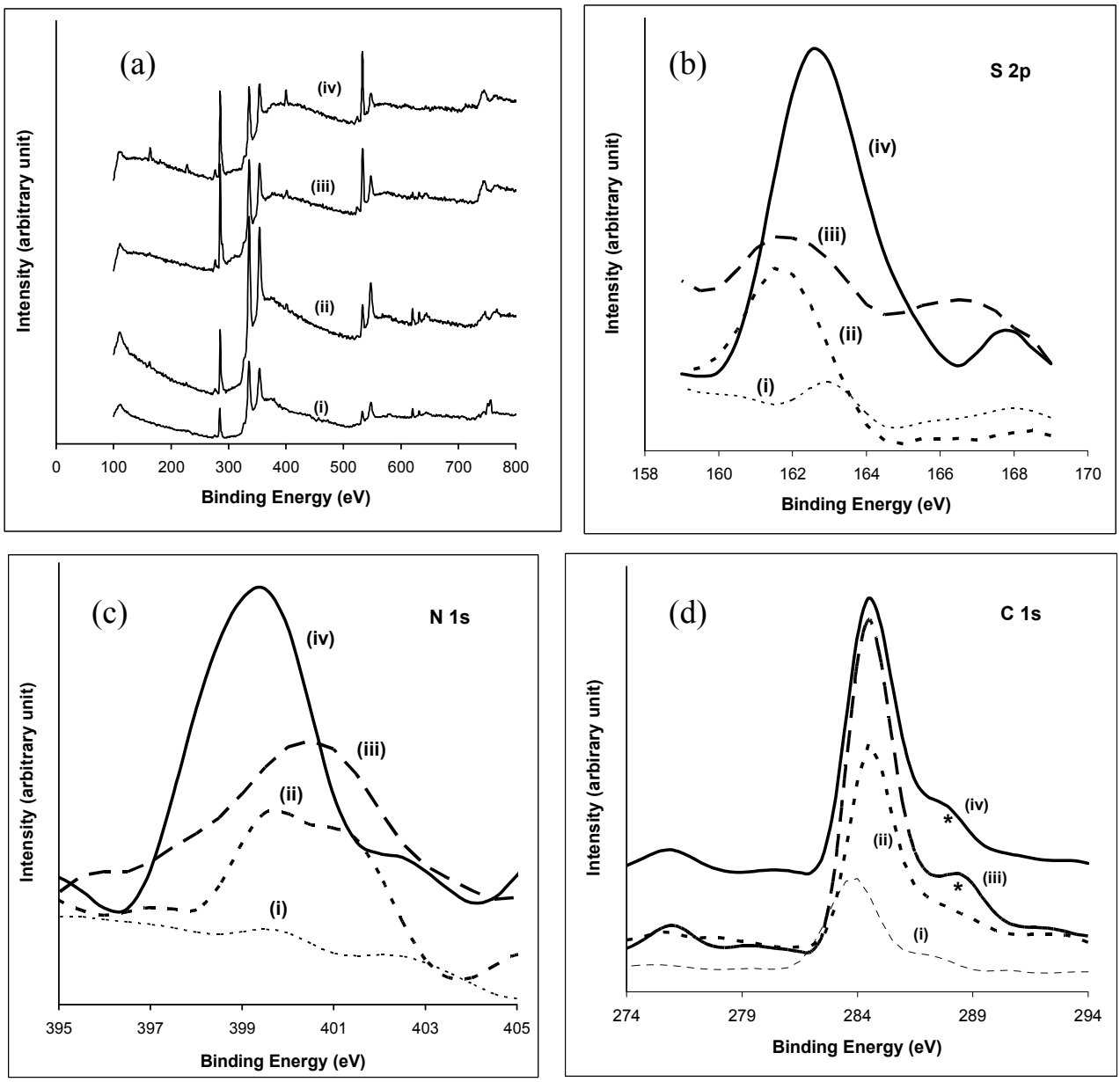

Figure 3.2: Survey X-ray photoelectron spectra for the full (a) and the expanded regions for the sulphur (b), nitrogen (c) and carbon (d) for the bare Au (i), Au-Cys (ii), Au-Cys-SWCNT (iii), and Au-Cys-SWCNT-FeOHETPc (iv) electrodes.

The 1 eV shift of the sulphur (2p) peak of the Au-Cys-SWCNT-FeOHETPc with increased peak intensity (Figure 3.2(b) (iv)) compared to those of the other SAMs suggest the presence of both gold bound (Au-S) and the sulphur of the peripheral substituents (-S$(CH_2)_2$OH) of the FeOHETPc species. The presence of these two types of sulphur for the Au-Cys-SWCNT-FeOHETPc was confirmed by a multiplexing experiment which revealed two peaks at ~161.5 and 162.7 eV for the Au-Cys-SWCNT-FeOHETPc and one peak at ~161.5 eV for the Au-Cys SAM. The cysteamine SAM showed two components for the nitrogen (1s) peak at 399.5 and 401 eV, which is in agreement with literature for cysteamine SAMs [9]. The nitrogen (1s) peak for the phthalocyanine is known to occur at either 398 or 400 eV [10], thus the appearance of sharp nitrogen (1s) peak for the FeOHETPc at 399.5 eV confirms the attachment of the FeOHETPc on the SWCNT. The nitrogen (1s) peak of the CONH for the SWCNT was observed at 400.5 eV. The different binding energies for the nitrogen (1s) of the different SAMs is indicative of the different environments where the nitrogen atoms occur. As would be expected, in terms of peak intensity and binding energy width, SWCNT exhibited relatively high concentrations of carbon Figure 3.2(d) (iii) and oxygen (not shown). Also, unlike the cysteamine SAM (Figure 3.2(d) (ii)), the SWCNT (Figure 3.2(d) (iii)) and FeOHETPc (Figure 3.2(d) (iv)) SAMs exhibited

shoulders in the binding energy regions of 287.5 and 289.5 eV (see asterisked), attributed to the carbonyl and carboxylic groups [10,11] and suggesting the formation of the amide and ester bonds during the self-assembly. The Au-Cys-SWCNT-FeOHETPc exhibited a weak peak at the binding energy of ~ 718 eV (not shown) corresponding to the Fe(II) peak (Fe, $2p^{3/2}$) [12].

3.4 Cyclic voltammetric characterization

3.4.1 Pretreatment of SWCNT-FeOHETPc

Unless otherwise stated, adsorption times of 18, 24 and 48 hr were adopted for the formation of the SAMs of Cys, SWCNT and FeOHETPc, respectively. It was dicovered that these SAMs could be formed within 8hr adsorption period; however, longer adsorption time was employed to permit for enhanced coverage of the SAMs on gold surface. To avoid possible oxidative desorption of the SAMs at high positive potential > 1.0 V vs Ag|AgCl, all voltammetric studies were restricted to the -0.20 to 1.0 V potential window. Previous studies [13,14] have shown that the first cyclic voltammetric scan of SAMs, especially the MPc SAM, sometimes differ from subsequent scans.

Figure 3.3 presents cyclic voltammetric profiles of the various electrodes studied compared with the bare Au in 0.5M H_2SO_4. The modified electrode exhibited strong electrochemical stability, confirmation proved by reproducibility in 0.5M H_2SO_4 solution during repetitive scanning. Such stability is important for electrochemical studies and application of surface-confined thin films in aqueous solutions.

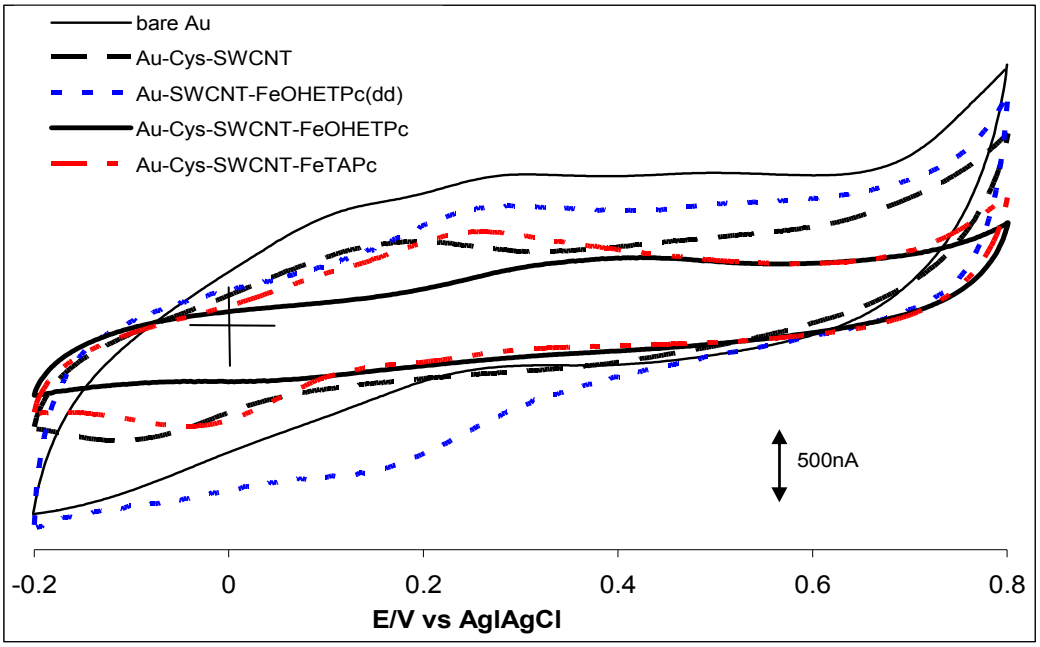

Figure 3.3: Cyclic voltammetric profile of the various electrodes studied, compared with the bare Au in 0.5 M H_2SO_4 at the scan rate of 25 mV s-1. Other scans heve been excluded for clarity.

The redox couple observed for the Au-Cys-SWCNT is attributed to the four-electron process [15]. From the several reports on the electrochemistry of surface-confined phthalocyaninatoiron(II) complexes [16-18], the peaks at the +0.23V and +0.02V at the A-Cys-SWCNT-FeOHETPc electrodes were attribute to the Fe(III)/Fe(II) redox process. For the SWCNT and SWCNT-FeOHETPc films, the peak separations are greater than the ideal zero volts expected for surface-

immobilized species which may be attributed to the kinetic limitations or some electrostatic interactions of the molecules in the films.

3.4.2 Interfacial capacitance

The interfacial capacitances of the films were estimated from the non-Faradaic region of the CVs (~ +0.6V vs Ag|AgCl)) using the equation (3.1) [18,19]:

$$C_T = \frac{I_{ch}}{\nu A} \qquad (3.1)$$

where C_T= total capacitance, I_{ch} = charging current, ν = scan rates and A is the area of the electrode. The capacitances estimated from Figure 3.3 were 1.4 μFcm^{-2} (bare gold), 0.6 μFcm^{-2} (Au-Cys), 0.7 μFcm^{-2} (Au-Cys-SWCNT), 0.6 μFcm^{-2} (Au-Cys-SWCNT-FeOHETPc), 1.2 μFcm^{-2} (Au-SWCNT$_{dd}$-FeOHETPc), 0.7 μFcm^{-2} (Au-Cys-SWCNT-FeOHETPc$_{(no\ DCC),}$) 0.6 μFcm^{-2} (Au-Cys-FeOHETPc), and 0.5 μFcm^{-2} (Au-FeOHETPc). Au-SWCNT$_{dd}$-FeOHETPc obtained by first preparing a nanotube bed by drop-coating SWCNT gave good FeOHETPc electrochemistry but with huge capacitive current. Various reports [20-22] have indicated that the electrochemistry of small redox-active molecules and proteins were observed through hydrophobic walls of CNTs. Also phthalocyanine complexes such as tetra-*tert*-butylphthalocyanines [23], FePc [24] and CoTAPc [25] have been

observe to strongly adsorb onto CNT via π-π interactions. Thus, the observed electrochemistry of FeOHETPc on SWCNT bed electrode as seen in figure 3.3 should perhaps not be surprising as the bed position could easily allow direct association of the phthalocyanine ring of the FeOHETPc with the walls of the SWCNT via π-π interaction (although some covalent interactions cannot be completely ruled out). Note also that some electrochemistry of the FeOHETPc is observed at the Au-Cys-SWCNT-FeOHETPc in the absence of DCC, which is necessary for covalent linkages of the SWCNT and FeOHETPc. This indicates that there is significant non-specific adsorptions of the FeOHETPc on the SWCNT, the same explanation of close π-π interaction as for the bed position could also hold for this behaviour. The relatively smaller capacitive current of the Au-Cys-SWCNT-FeOHETPc, coupled to the faster electron transfer kinetics (further discussed in section 3.5) is advantageous to electroanalytical applications and underscores the preference of the aligned nanotube compared to electrode without DCC or its bed form on gold electrode.

The results obtained here is consistent with literature precedents where the capacitance of bare Au is usually more than order of maginitude higher than the typical capacitances for most alkanethiol SAMs [18,19]. The marked decreased in the capacitive charging currents of the bare gold electrode by the modifying species is

characteristic of compact and less defective films capable of suppressing electrolyte ions from penetrating into the film. The ability of the films to suppress ion penetration increases with increasing hydrophobicity of the film head groups (which in this study are the –NH_2 for cysteamine; –COOH for the SWCNT, and –OH for the FeOHETPc). Based on the p*Ka* of the head groups of the species used in this work mercaptoethanol 9.5; [26] cysteamine (10.5) [26,27] and benzyl species substituted with carboxylic group (in the 4.0–5.0 [28,29]), it suggests that their ion suppression ability should follow the observed trend of Cysteamine ≈ FeOHETPc > SWCNT. The capacitance values of various SWCNT-modified electrodes obtained by dip-coating were reported to fall in the 159–710 $\mu F/cm^2$ range [30-33]. The difference between these data and the results from this thesis is that dip-coated SWCNTs give much higher coverage compared to the self-assembly method [34]. Thus, the high capacitance for the Au-SWCNT-FeOHETPc obtained in this work is attributed to the higher amount of SWCNT on the Au obtained by drop-dry method. Also, these results differ from reports in 0.01 M PBS pH 4.4 or 1.0 M Na_2SO_4 pH 4.0 [13,14] where the SAMs exhibited higher capacitive currents than the bare Au. This deviation may be associated with the working electrolytes (0.5 M H_2SO_4) used in this study. This prompted us to carry out all the studies in this electrolyte conditions. Advantageously,

this electrolyte condition also activates the central Fe(II)/Fe(III) redox process of the attached FeOHETPc species compared to PBS pH 4.4.

3.4.3 Surface coverage

The amounts of the SAM molecules on the gold surface (Γ) were estimated from the anodic charges of the CV profiles in 0.5 M H_2SO_4 (Figure 3.3) using the expression [18,19,35]:

$$\Gamma_{SAM} = \frac{Q}{nFA} = \frac{\int Idt}{nFA} \qquad (3.2)$$

where Q is the background-corrected charge under the cathodic or anodic waves, n = number of electrons involved in the redox process, F is the Faraday constant (96485 C mol^{-1}), and A is the experimentally determined area of the electrode. Assuming a four-electron for the Au-Cys-SWCNT redox process, [15] and one-electron process for the other electrodes, the surface concentrations were approximately as 6.8 x 10^{-10} mol cm^{-2} (*ca* 4.1 x 10^{14} molecules cm^{-2} or ~ 24 $Å^2$ per molecule) for the Au-Cys, 1.4 x 10^{-10} mol cm^{-2} (*ca*. 8.2 x 10^{13} particles cm^{-2} ≈ 122 $Å^2$ per particle) for the Au-Cys-SWCNT, and 7.0 x 10^{-10} mol cm^{-2} (*ca* 4.2 x 10^{14} molecules cm^{-2} or ~ 24 $Å^2$ per molecule) for the Au-Cys-SWCNT-FeOHETPc. The values are of similar magnitudes as those reported in the literature for the Au-Cys [3,4], Au-Cys-SWCNT [3,4], and Au-FeOHETPc [13], confirming monolayer coverage [18,19]. The

similarity in surface coverages suggests that the observed electrochemistry was due to the SWCNT attached to the cysteamine, and FeOHETPc attached to the ends of the SWCNTs. The projected area of the FeOHETPc molecule (assuming a diameter of ~ 20 $Å^2$ as discussed in the AFM results above [6]) is ~315 $Å^2$, implying that for this MPc to lie flat on the ends of the SWCNTs, then its coverage should work out to be ~ 3.2 x10^{13} particles cm^{-2}, i.e. ~ 5.3 x10^{-11} mol cm^{-2}. Thus, the high surface coverage for the FeOHETPc is a clear confirmation of a standing position rather than flat orientation, corroborating the AFM results for the FeOHETPc. Interestingly, FeOHETPc is also known to prefer perpendicular orientation when adsorbed on a gold surface as a SAM [13]. Similarly, the cross sectional area for a single SWCNT of diameter of ~ 1.3 nm [4] should be *ca*. (1.33 – 1.54) x 10^{-14} cm^{-2}, meaning that each SWCNT particle occupies an area of ~133 – 154 $Å^2$, which is in close correlation with the surface coverage (~122 $Å^2$) obtained in this work. This result is consistent with the AFM results which showed that these SAMs lie normal to the gold surface. The surface concentrations shown by other FeOHETPc-based electrodes also indicate horizontal rather than vertical orientations. The coordination of Cys with FeOHETPc could occur via axial ligation of the $–NH_2$ with the central Fe [35] and/or electrostatic attraction. Axial ligation (flat orientation) is excluded as

the surface coverage would have been smaller than the observed value. For the other electrodes, the surface concentrations were estimated as 4.2 x 10^{-10} mol cm^{-2} (Au-FeOHETPc, 1.2 x 10^{-9} mol cm^{-2} (Au-Cys-SWCNT-FeOHETPc$_{(no\ DCC)}$) and 4.5 x 10^{-9} mol cm^{-2} for the Au-SWCNT$_{dd}$-FeOHETPc. The coverage of the randomly dispersed nanotubes or the bed form (Au-SWCNT$_{dd}$-FeOHETPc) is about 40 times greater than those obtained by the aligned nanotubes (Au-Cys-SWCNT-FeOHETPc). Surface-confined electropolymeric complexes of redox-ctive of MPc complexes give coverages in the 10^{-9} and 10^{-8} mol cm^{-2} order, thus this result suggests that the Au-SWCNT$_{dd}$-FeOHETPc could be acting like a redox polymer rather than a monolayer.

3.5 Electrochemical impedimetric characterization

3.5.1 Electron transport behaviour of the SAMs

Cyclic voltammetric and impedimetric responses of the different electrodes in aqueous solution of the outer-sphere redox probe, $[Fe(CN)_6]^{3-}/[Fe(CN)_6]^{4-}$ were compared as emplified in figure 3.4 (CV) and figure 3.5 (EIS). Impedance spectroscopy was used since it is well-recognized as a powerful diagnostic tool for providing high accuracy in measuring the electron transport properties of redox-active SAMs [37-40]. Therefore, in figure 3.5 we see the Nyquist plots which exhibit the characteristic semicircles at high frequencies and a straight line at low frequencies, corresponding to kinetic and diffusion processes, respectively.

The phase angles seen in figure 3.6(a) (i.e., –phase angle *(ϕ)* vs log *f*,) are in the range of 30 - 40°, which are less than the 90° expected of an ideal capacitive behaviour. The lower the phase angle, the lower the capacitive behaviour of the electrode hence the faster the electron transfer.

The other Bode plot illustrates the relationship between the logarithm of impedance and frequency. The slopes of the Bode plots (log *Z* vs log *f*) are approximately similar for all the electrodes (*ca*. –0.37, r^2 = 0.996) at the mid frequency region, indicative of

pseudocapacitive behaviour. At high frequency regions, the slopes are almost zero, indicative of resistive behaviour at these high frequency regions.

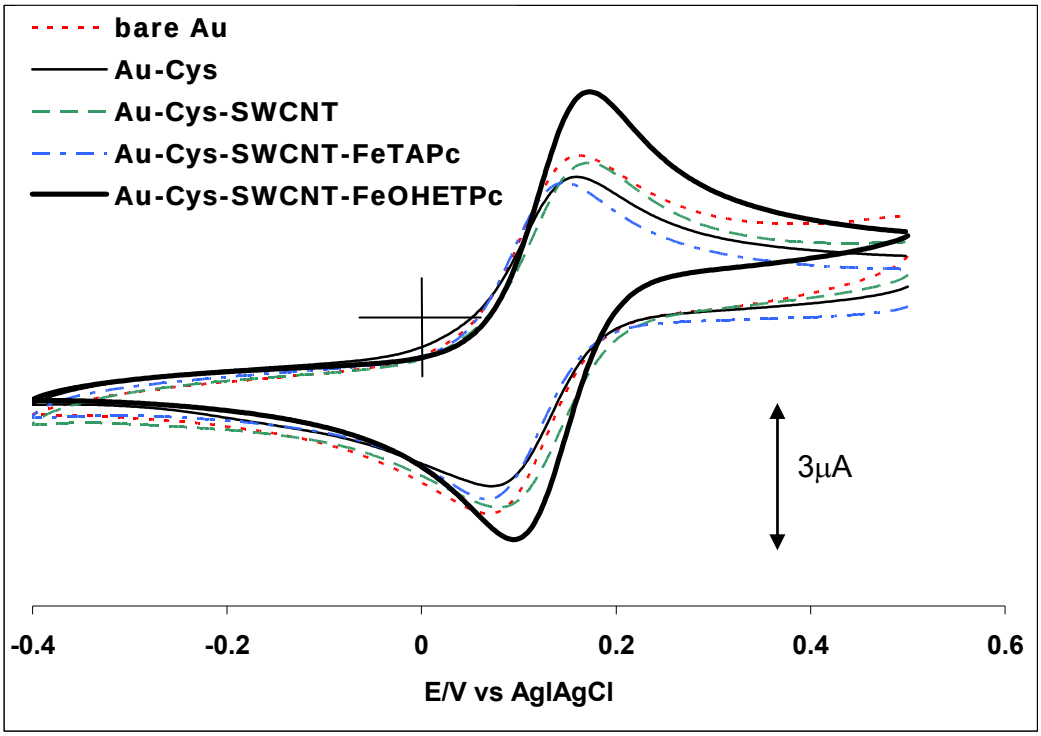

Figure 3.4: Typical cyclic volammograms of the indicated electrodes towards the reversible couple $Fe(CN)_6]^{3-}$/ $[Fe(CN)_6]^{4-}$ in 0.1 M PHS (pH 4.8). scan rate: 25 mVs^{-1}.

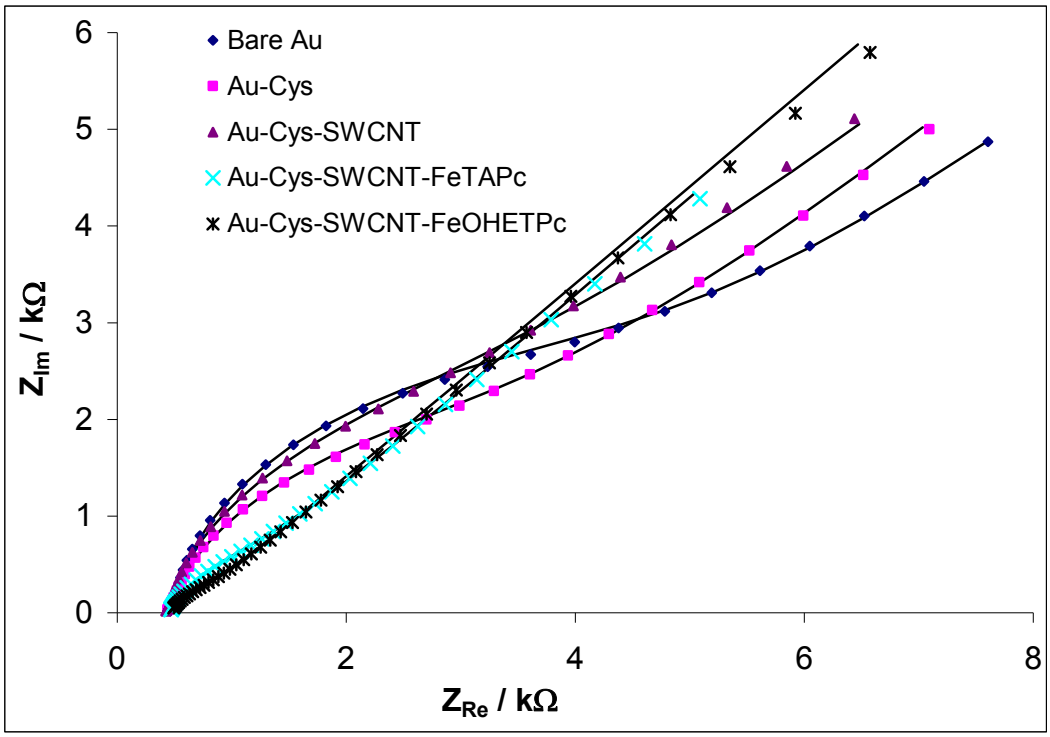

Figure 3.5: Impedance spectral responses of the indicated electrodes obtained at +0.10 V vs AglAgCl in $Fe(CN)_6]^{3-}$/ $[Fe(CN)_6]^{4-}$ 0.1 M PBS (pH 4.8)

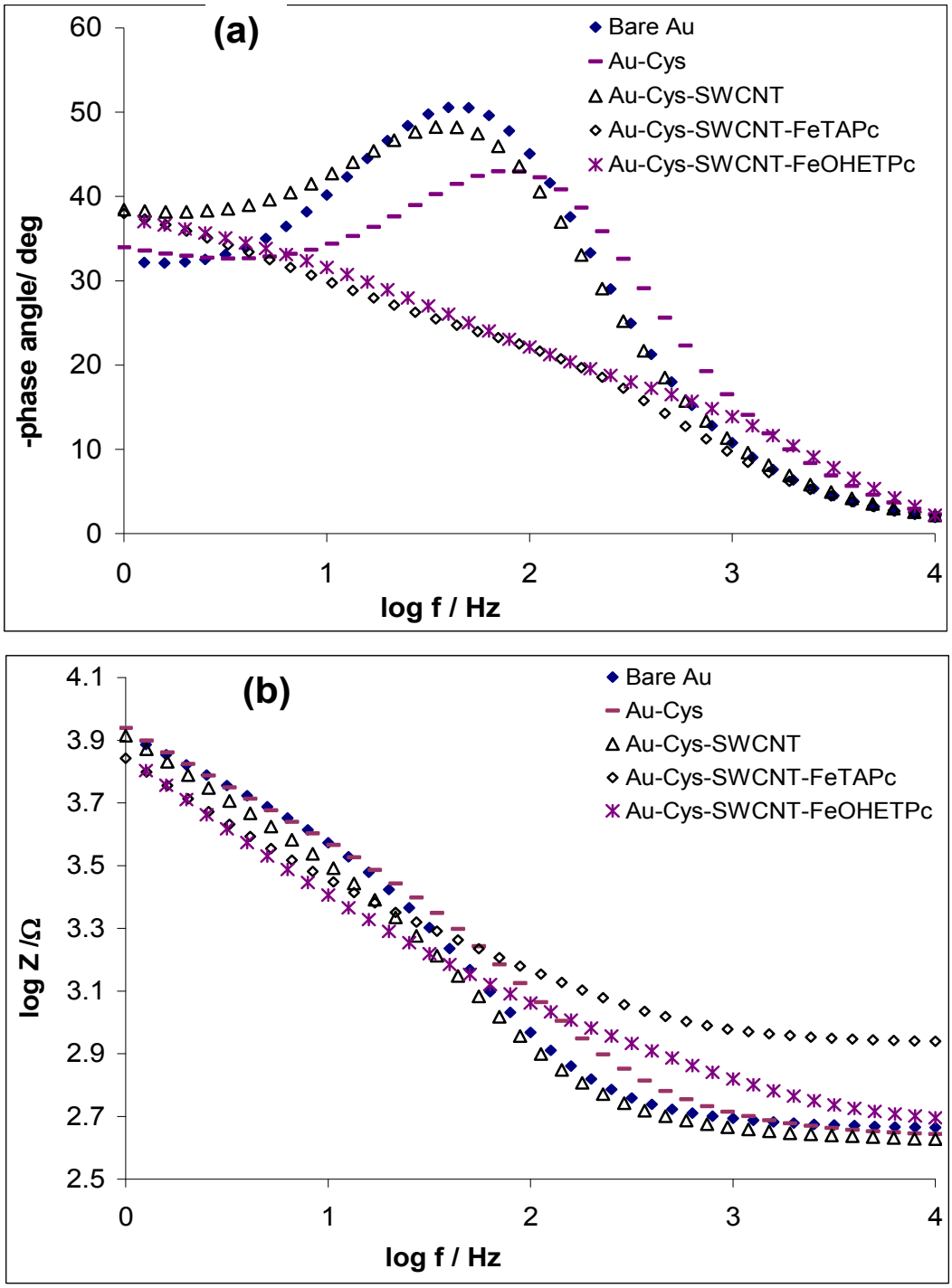

Figure 3.6: Bode plots, phase angle vs log f (a) and log Z vs log f (b),of the impedance spectra of the modified electrodes in redox probe ($[Fe(CN)_6]^{4-}$/ $[Fe(CN)_6]^{3-}$) in 0.1 M PBS solution (pH 4.8).

3.5.2 Impact of solution pH on electron transfer

The effects of solution pH and estimation of the surface *pka* values of SAM-modified electrodes are important in the theory and potential applications of the SAMs [41-46]. The *pka* of a surface-confined species is defined as the value of the pH in contact with the monolayer when half of the functional groups are ionized [46]. The *pka* of Au-Cys SAM has been reported to be ~7.6 and so was not repeated in this report. Figure 3.7 presents examples of the plots of R_{CT} vs pH for the Au-Cys-SWCNT (A) and Au-Cys-SWCNT-FeOHETPc (B) in PBS solutions of $[Fe(CN)_6]^{3-/4-}$.

The differences in the impedance spectral profiles indicate the coordination of the different SAMs with different head groups giving different surface reactions. With increasing pH, the R_{CT} values markedly increase, which could be ascribed to the increasing dissociation/deprotonation of the monolayer head groups. Each of the electrodes exhibits semicircles in the high frequency region and a Warburg line in the low frequency region even at pH $\geq$ 9.0, suggesting that semi-infinite diffusion process still occurs at this high pH.

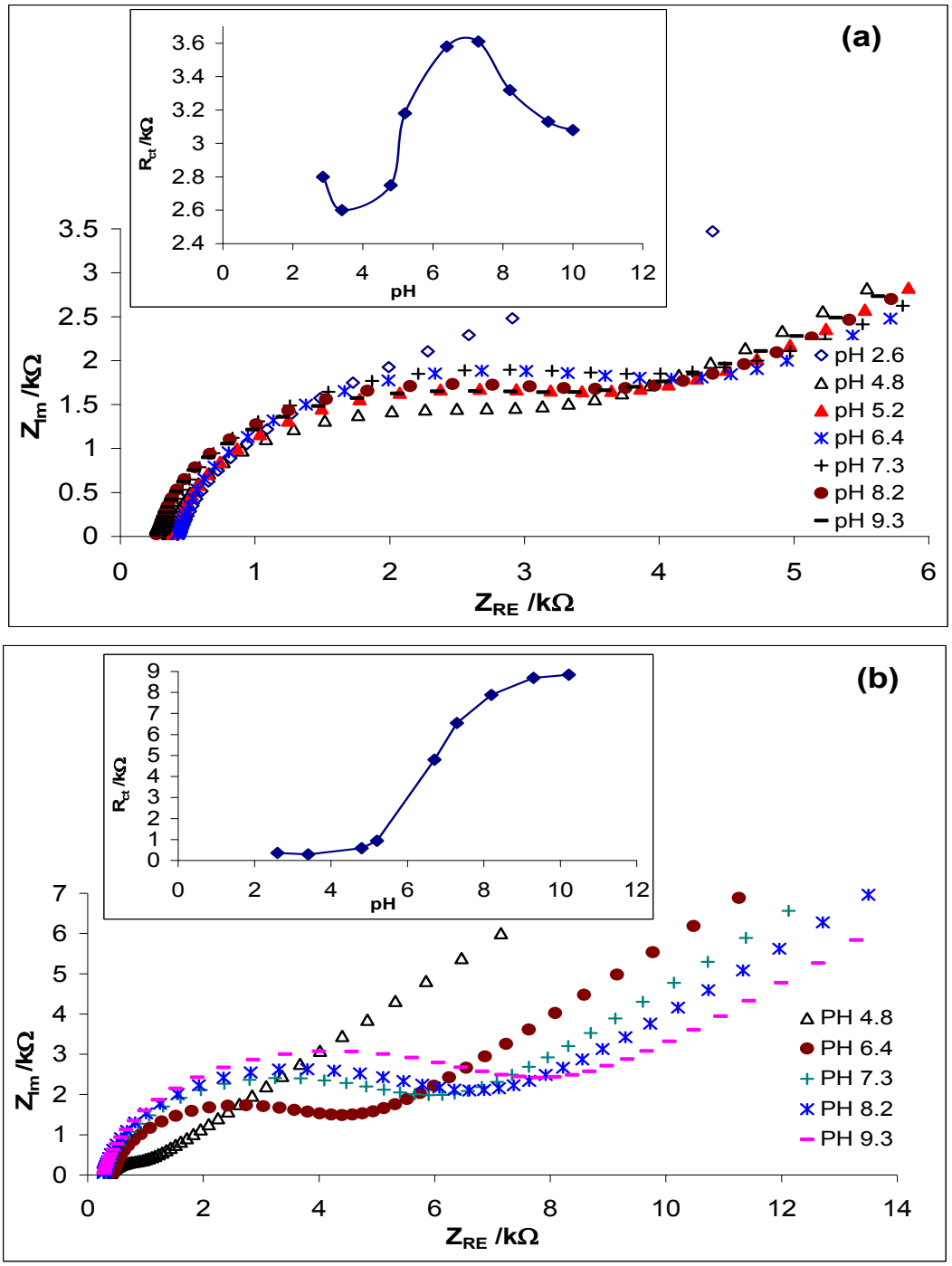

Figure 3.7: Examples of the impedimetric responses of the Au-Cys-SWCNT (a) and Au-Cys-SWCNT-FeOHETPc (b) at different pH of the $Fe(CN)_6]^{3-}$/$[Fe(CN)_6]^{4-}$ solutions. Insets are the corresponding plots of R_{CT} vs pH.

This behaviour should make some sense considering (i) that the solution p*Ka* values of mercaptoethanol (for the Au-Cys-SWCNT-FeOHETPc electrode) is 9.5 [26]; and (ii) that the –COOH group and other functionalities as the phenols present in acid digested SWCNTs are stabilized by the strong hydrogen bonding that could impede the facile ionization of the Au-Cys-SWCNT. The increase in the R_{CT} of the Au-Cys-SWCNT at pH ≥ 5 is due to the electrostatic repulsion of the anionic probe by the negative potential established at the monolayer -COOH head group. At pH ≥ 7.5, the electron transport slightly increases, possibly due to repulsive interations of the fully ionised neighbouring head groups that could lead to less compactness of the SAM and permit the penetration of the redox probe into the underlying electrode, a similar phenomenon that had been observed for SAMs by Jun and Beng [47]. The surface *pKa*s of the electrodes could be estimated from the midpoints of the R_{CT} vs pH plots. We estimated the surface p*Ka* for the Au-Cys-SWCNT to be *ca.* 5.5. Back and Shim [48] reported the pH-responsiveness of a single isolated SWCNT electrochemical transistor integrated with microfluidic channel under 10 mM KCl solution and found that the threshold voltage shifted with pH while its transconductance and subthreshold swing remained independent of pH. From the plot of the threshold shift (ΔV_t / V) with pH, a p*K*a value of ~ 7.6 was estimated. Given that the experimental

conditions employed by these authors are widely different, it is impossible to adequately compare the findings in this present work with theirs. For example, the authors studied a single isolated SWCNT (not treated in acid conditions, meaning it has little or no -COOH) in unbuffered electrolyte with high ionic strength. It is interesting to read from the recent work of Yang *et al*. [49] that SWCNT containing a large number of carboxyl groups (SWCNT grafted with polyacrylic acids) exhibit strong responses only at below or above pH 5. The *pKa* of the Au-Cys-SWCNT-FeOHETPc was estimated to be *ca.* 7.3. This value is slightly lower than the *pKa* value of the mercaptoethanol solution of 9.5 [26], this difference may be attributed to the stabilizing effect of the resonating sp^2 carbons of the phthalocyanine rings to which the mercaptoethanol moiety is attached.

3.5.3 Impact of single-walled carbon nanotubes on electron transfer

The FeOHETPc-based electrodes gave higher electron transfer at acidic conditions (see pH studies above), in good agreement with previous studies where it was established that MPc SAMs gave better electrochemical response in pH < 7 [13,14]. Hence, in this present work, the electron transport properties of all the modified electrodes at acidic conditions were compared. Fig 3.8(a) presents a comparative

Nyquist plots of (i) bare Au, (ii) Au-FeOHETPc, (iii) Au-Cys-SWCNT, (iv) Au-Cys-FeOHETPc, (v) Au-Cys-SWCNT-FeOHETPc$_{(No\ DCC)}$, (vi) Au-Cys-CoTAPc, and (vii) Au-Cys-SWCNT-FeOHETPc in 0.1 M PBS (pH 4.8). Other electrodes have been removed from the figure for clarity purposes but their impedance spectral data are summarized in Table 3.1. The experimental EIS data was fitted with the equivalent circuit of mixed kinetic and diffusion control (Figure 3.8(b)) involving a solution resistance, R_s, in series with Q which is a measure of capacitance of the constant phase element, CPE, R_{CT} is the electron-transfer resistance (domain of kinetic control) and Z_w is the Warburg impedance (domain of mass transport control) resulting from the diffusion of ions to the electrode interface from the bulk of the electrolyte. The impedance of the CPE (Z_{CPE}) is a power-law dependent interfacial capacity given as:[40]

$$Z_{CPE} = [Q(j\omega)^n]^{-1} \qquad (3.3)$$

where Q is the frequency-independent constant, ω is the radial frequency, and n is an exponent related to the depression angle. An n value of zero corresponds to a pure resistor; a unit value of n corresponds to a pure capacitor. The CPE model was chosen for simulating the EIS data to represent the real world situation that recognizes the topographic imperfections or roughness of the electrode.

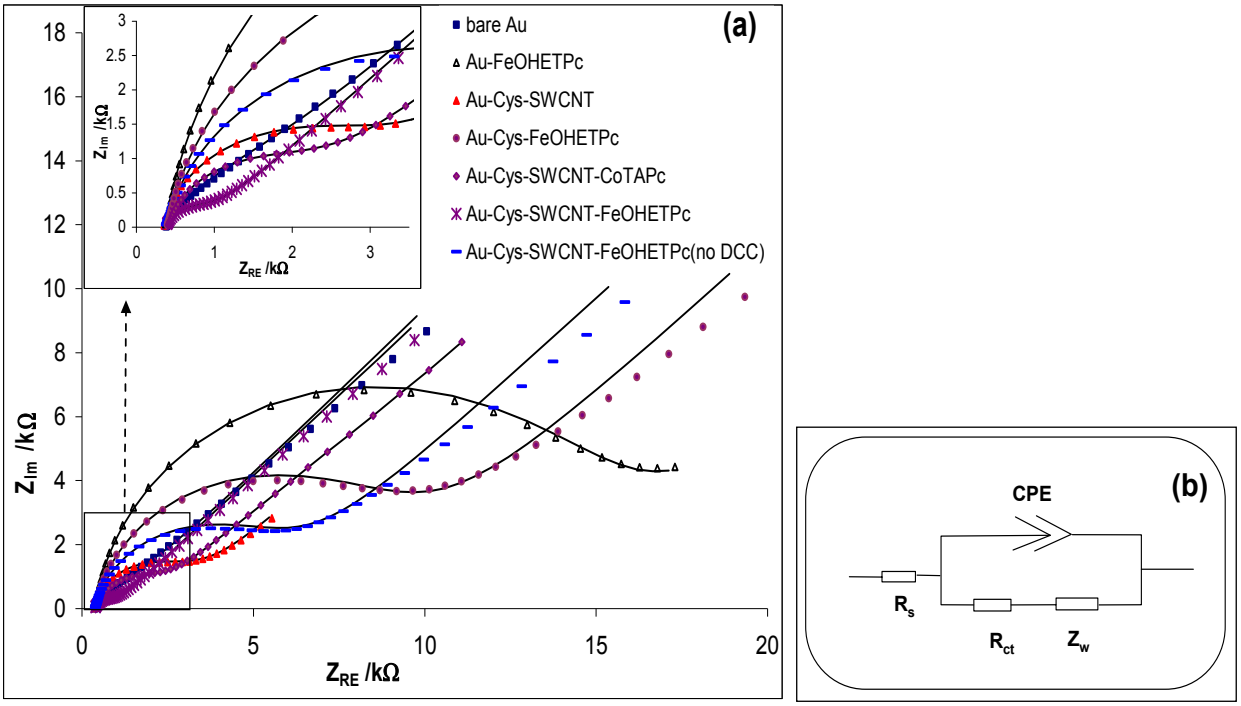

Figure 3.8: Examples of comparative Nyquist (a) and circuit used (b) fot the different modified electrodes in 0.1 M PBS (pH 4.8). Others have been removed for clarity but the EIS data are shown in Table 3.1.

As can be seen in the Table, the EIS data adequately fitted the chosen equivalent circuits with low estimated percentage errors (R_s in the 0.4 – 0.8% range; Q in the 3 – 13% range; R_{CT} between 1 and 10%; Z_w between 0.4 and 6% and n between 0.3 and 1.6%). As expected, n values extracted from the equivalent circuit were in the 0.6 – 0.9 range, confirming that the electrodes exhibit pseudocapacitive behaviour. Note that the Q values obtained here are consistent with the C_T estimated from the voltammetric analysis in equation 1, the electrode obtained by randomly dispersing SWCNT on

the gold electrode (Au-Cys-SWCNT$_{dd}$-FeOHETPc) gave the highest Q values. It is interesting to observe that the Q value for the Au-Cys-SWCNT$_{dd}$-FeOHETPc is about 30 times greater than of the aligned Au-Cys-SWCNT-FeOHETPc electrode.

Also, the comparative Bode plots of phase angle vs log *f* (Figure 3.9 (a)) showed well-defined symmetrical peaks at different maxima for the different electrodes, corresponding to the different relaxation processes of the electrode|solution interfaces. The slopes of the Bode plots (log *Z* vs log *f*, Figure 3.9(b)) are approximately identical for all the electrodes (*ca*. –0.40, r^2 = 0.997) at the mid frequency region, indicative of pseudocapacitive behaviour. At high frequency regions, the slopes are almost zero, indicative of resistive behaviour at these high frequency regions. The phase angles (i.e., –phase angle *(ϕ)* vs log *f*,) which are in the range of 25 - 42^o, less than the 90^o also expected of an ideal capacitive behaviour.

The apparent electron transfer rate constant k_{app} was obtained from the conventional equation [50] (see Table 3.1):

$$k_{app} = \frac{RT}{n^2 F^2 A R_{CT} C} \qquad (3.4)$$

where n is the number of electron transferred (i.e. n=1), A is the geometric area of the electrode (0.027 cm^2), C is the concentration of the $[Fe(CN)_6]^{3-}$ (in mol cm^{-3}, the concentration of $[Fe(CN)_6]^{3-}$ and

$[Fe(CN)_6]^{4-}$ are equal), R, T and F have their usual meanings. As exemplified in the acidic pH, FeOHETPc without SWCNT showed much higher R_{CT} value (low k_{app}) than the SWCNT-FeOHETPc, indicating that SWCNT markedly enhances the electronic communications between FeOHETPc and the gold electrode. It is also noteworthy here to observe (Figure 3.8, pH 4.8 PBS) that under similar experimental conditions employing $[Fe(CN)_6]^{3-/4-}$ as redox probe, Au-Cys-SWCNT-FeOHETPc showed much faster electron transfer (~ 3 times faster) than the previously reported Au-Cys-SWCNT-CoTAPc. Thre is no firm explanation for this but may be related to the differences in the head groups and central metal ions that change the chemistry of the two MPc complexes. Depending on experimental conditions, surface-immobilized FePc complexes sometimes show faster electron transport and better catalysis compared to their surface-immobilised CoPc counterparts [51] The value of k_{app} for the Au-Cys-$SWCNT_{dd}$-FeOHETPc (~1.2×10^{-3} cm s^{-1}) is about 16 times less than that of the aligned Au-Cys-SWCNT-FeOHETPc electrode (~1.7×10^{-2} cms^{-1}). This is in good agreement with the report of Gooding and coworkers [3,52] that electron transfer to ferricyanide in solution was slower at randomly dispersed SWCNTs than at vertically aligned SWCNTs.

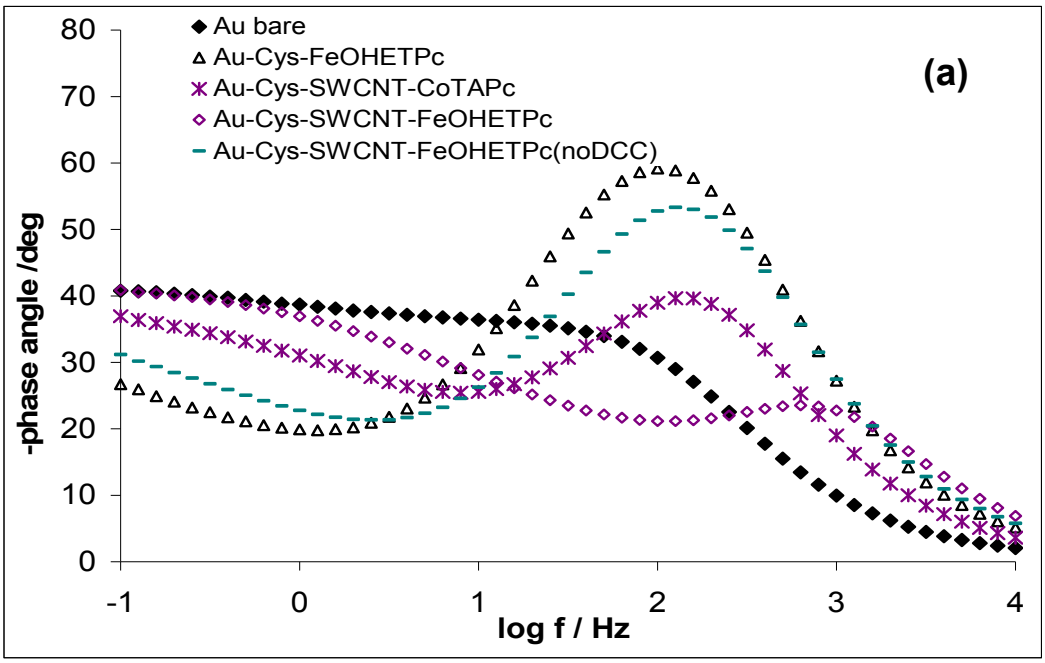

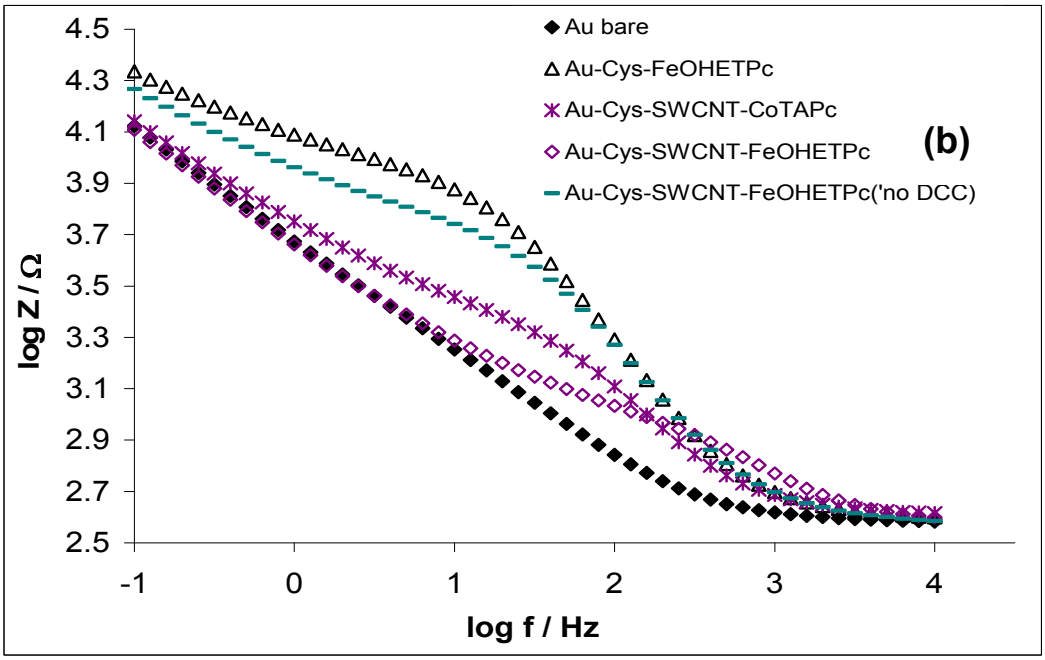

Figure 3.9: Bode plots, phase angle vs log f (a) and log Z vs log f (b),of the impedance spectra of the modified electrodes in redox probe ($[Fe(CN)_6]^{4-}$/ $[Fe(CN)_6]^{3-}$) in 0.1 M PBS solution (pH 4.8). Others have been removed for clarity but the EIS data are shown in Table 3.1.

This difference may be related to the different pathways to which electrons move at the two orientations. Unlike the vertically aligned orientation where electron-flow presumably occur between the underlying gold electrode and a redox species in solution through a single nanotube, at the randomly dispersed SWCNT, the electron-flow likely occur by hopping of electrons from one nanotube to the next mainly across the nanotube walls. Electron transport is expected to be faster along the tube than through the nanotube walls, similar to faster electron transport through edge plane than the basal plane [53,54]. Thus, electron hopping through nanotube walls should be expected to be the slowest step. Following similar literature reports for SWCNT-based SAM electrodes [3-5], the aligned SWCNTs may be assumed to act as efficient conductive nanowires in the electron transport process of the Au-Cys-SWCNT-FeOHETPc electrode.

Table 3.1: Summary of estimated EIS parameters.

Electrode	Estimated Electrochemical Impedance Parameter[1]					
	R_s / kΩ	Q / μF	R_{ct} / kΩ	10^4 Z_w / Ω $s^{-1/2}$	n	10^3 k_{app} / cm s^{-1}
Bare Au	0.38 (0.66)	0.42 (12.69)	1.92 (7.51)	9.02 (1.31)	0.75 (1.62)	5.14±0.39
Au-Cys	0.37 (0.66)	0.02 (11.38)	6.74 (7.76)	0.85 (4.98)	0.58 (1.04)	1.46±0.11
Au-Cys-SWCNT	0.36 (0.36)	0.52 (2.78)	2.75 (0.95)	1.05 (1.03)	0.97 (0.37)	3.59±0.03
Au-Cys-SWCNT-FeOHETPc	0.38 (0.83)	0.16 (11.82)	0.59 (2.75)	1.01 (0.36)	0.86 (1.64)	16.71±0.46
Au-$SWCNT_{dd}$-FeOHETPc[2]	0.39 (0.66)	4.83 (8.72)	8.55 (9.93)	0.99 (4.85)	0.83 (1.14)	1.15±0.11
Au-Cys-FeOHETPc	0.40 (0.62)	0.36 (3.23)	8.67 (0.95)	0.87 (1.31)	0.90 (0.38)	1.14± 0.01
Au-Cys-SWCNT-$FeOHETPc_{(no\ DCC)}$[3]	0.38 (0.75)	0.32 (4.50)	5.38 (1.26)	0.89 (1.21)	0.88 (0.55)	1.83 ±0.02
Au-FeOHETPc	0.76 (0.62)	0.31 (2.72)	4.81 (1.10)	1.00 (6.04)	0.92 (0.33)	0.67±0.01
Au-Cys-SWCNT-FeTAPc	0.91 (0.31)	2.34 (7.32)	0.95 (2.01)	1.04 (0.48)	0.86 (1.10)	0.28±0.02

[1]. The values in brackets for R_s, Q, R_{CT}, Z_W and n are the estimated error in percent. All potential were measured against Ag|AgCl wire. [2].Electrode obtained by first coating the gold electrode with SWCNT and drying, followed by immersion in DMF solution of FeOHETPc for 25h; [3].Electrode obtained without the addition of the coupling agent, DCC, in either the solution of SWCNT or FeOHETPc.

REFERENCES

1. K. I. Ozoemena, T. Nyokong, P. Westbroek, *Electroanalysis* 15 (2003) 1762.
2. M. P. Somashekarappa, J. Keshavaya, S. Sampath, *Pure Appl. Chem*. 74 (2002) 1609.
3. J. J. Gooding, R. Wibowo, J. Liu, W. Yang, D. Losic, S. Orbons, F. J. Meams, J. G. Shapter, D. B. Hibbert, *J. Am. Chem. Soc.* 125 (2003) 9006.
4. F. Patolsky, Y. Weizmann, I. Willner, *Angew. Chem. Int. Ed*. 43 (2004) 2113.
5. L. Sheeney-Haj-Ichia, B. Basnar, I. Willner, *Angew. Chem. Int. Ed*. 44 (2005) 78.
6. Z. Li, M. Lieberman, W. Hill, *Langmuir* 17 (2001) 4887.
7. B. Varughese, S. Chellama, and M. Lieberman, Langmuir 18 (2002) 7964.
8. C. -J. Zhong, R. C. Brush, J. Anderegg, M. D. Porter, *Langmuir* 15 (1999) 518.
9. M. Wirde, U. Gelius, L. Nyholm, *Langmuir* 15 (1999) 6370.
10. Z. Chen, K. Kobashi, U. Rauwald, R. Booker, H. Fan, W. -F. Hwang, J. M. *Tour, J. Am. Chem. Soc.* 128 (2006) 10568.
11. J. Chattopadhyay, F. de Jesus Cortez, S. Chakraborty, N. K. H. Slater, W. E. Billups, *Chem. Mater*. 18 (2006) 5864.

12. Handbook *of X-Ray Photoelectron Spectroscopy,* ed. G. E. Muilenberg, Perkin-Elmer Corp, Eden Praire, Minnesota, 1979.

13. K. I. Ozoemena, T. Nyokong, P. Westbroek, *Electroanalysis* 15 (2003) 1762.

14. K. I. Ozoemena, T. Nyokong, *Electrochim. Acta*, 47 (2002) 4035.

15. H. Luo, Z. Shi, N. Li, Z. Gu, Q. Zhuang, *Anal. Chem.* 73 (2001) 915.

16. A. B. P Lever, E. R. Milaeva, G. Speier In: A. P. B. Lever and C. C. Leznoff, Editors, *Phthalocyanines: Properties and Applications,* Vol.3, VCH Publishers, New York 1993.

17. M. P. Somashekarappa, J. Keshavaya, S. Sampath, *Pure Appl. Chem*. 74 (2002) 1609.

18. H. O. Finklea in *Electroanalytical Chemistry,* eds. A. J. Bard and I. Rubinstein, Marcel Dekker, New York, Vol. 19, 1996, p.109.

19. H. O. Finklea in *Encyclopedia of Analytical Chemistry: Applications, Theory and Instrumentations,* eds. R.A. Meyers, Wiley, Chichester, 11 (2000) 10090.

20. J. K. Campbell, L. Sun, R. M. Crooks, *J. Am. Chem. Soc*. 121 (1999) 3779.

21. B. R. Azamian, J. J. Davis, K. S. Coleman, C. B. Bagshaw, M. L. H. Green, *J. Am. Chem. Soc*. 124 (2002) 12664.

22. M. Shin, N. W. S. Kam, R. J. Chen, Y. M. Li, H. J. Dai, *Nano Lett*. 2 (2002) 285.

23. X. Wang, Y. Liu, W. Qiu, D. Zhu, *J. Mater. Chem.* 12 (2002) 1636.

24. J. S. Ye, Y. Wen, W. D. Zhang, H. F. Cui, G. Q. Xu, F. S. Sheu, *Electroanalysis* 17 (2005) 89.

25. K. I. Ozoemena, J. Pillay, T. Nyokong, *Electrochem. Commun*. 8 (2006) 1391.

26. H. Munakata, D. Oyamatsu, and S. Kuwabata, *Langmuir* 20 (2004) 10123.

27. R. Z. Shervedani, M. Bagherzadeh, and S. A. Mozaffari, *Sens. Actuators B* 115 (2006) 614.

28. C. R. Raj and S. Behera, *J. Electroanal. Chem*. 581 (2000) 61.

29. J. Ye, J. Liu, Z. Zhang, J. Hu, S. Dong, Y. Shao, *J. Electroanal. Chem*. 508 (2001)123.

30. H. Luo, Z. Shi, N. Li, Z. Gu, Q. Zhuang, *Anal. Chem.* 7 (2001) 915.

31. M. Musameh, J. Wang, A. Merkoci, Y. Lin, *Electrochem. Commun*. 4 (2002) 743.

32. J. Wang, M. Li, Z. Shi, N. Li, Z. Gu, *Electroanalysis* 14 (2002) 225.

33. L. Wang, J. Wang, F. Zhou, *Electroanalysis* 16 (2004) 627.

34. L. Su, F. Gao and L. Mao, *Anal. Chem*. 78 (2006) 2651.

35. A. J. Bard, L. R. Faulkner, Electrochemical Methods: Fundamentals and Applications, 2nd ed., John Wiley & Sons, Hoboken, NJ. 2001

36. G. Kalyuzhny, A. Vaskevich, G. Ashkenasy A. Schanzer, I. Rubinstein, *J. Phys. Chem. B*. 104 (2000) 8238.

37. E. Kats and I. Wilner, Electroanalysis 15 (2003) 913.

38. E. Kats and I. Wilner in: V. M. Mirsky (Ed.), Ultrathin Electrochemical Chemo and Biosensors. Technology and Performance, Springer-Verlag, New York, Chapter 4 (2004) 68

39. E. Barsoukov, J. R. Macdonald (Ed.), Impedance Spectroscopy: Theory Experiment and Applications 2nd ed., Wiley Hoboken, New Jersey, Chapter 1-4 (2005)

40. D. D. Macdonald, Electrochim. Acta 51 (2006) 1376.

41. M. A. Bryant and R. M. Crooks, Langmuir 9 (1993) 385.

42. J. Zhao, L. Luo, X. Yang, E. Wang, and S. Dong, *Electroanalysis* 11 (1999) 1108.

43. J. F. Smalley, K. Chalfant, S. W. Feldberg, T. M. Nahir, and E. F. Bowden, J. Phys. Chem. B 103 (1999) 1676.

44. Y. Jiang, Z. Wang, H. Xu, H. Chen, X. Zhang, M. Smet, W. Dehaem, Y. Hirano and Y. Ozaki*, Langmuir* 22 (2006) 3715.

45. M. Root and A. M. Shaw, *Phys.chemChem.Phys*. 8 (2006) 4741.

46. T. R. Lee, R. D. Carey, H. A. Biebuyck, G. M. Whitesides, *Langmuir* 10 (1994) 741.

47. Y. Y. Jun, K. S. Beng, *Electrochem. Commun.* 6 (2004) 87.

48. J. H. Back and M. Shim, *J. Phys. Chem. B*. 110 (2006) 23736.

49. D. Yang, J. Hu, C. Wang, *Carbon* 44 (2006) 3161.

50. E. Sabatani, I. Rubinstein, *J. Phys. Chem.* 91(1987) 6663.

51. K. I. Ozoemena, T. Nyokong, In Encyclopedia of Sensors, C. A Grimes, E. C. Dickey, M. V. Pishko, Eds., American Scientific Publishers, California, 3 (2006) Chapter E, pp.157 – 200, and references therein.

52. J. J. Gooding, *Electrochim. Acta*. 50 (2005) 3049.

53. C. E. Banks, R. R. Moore, T. J. Davies, R. G. Compton, *Chem. Commun*. 2004 1804.

54. C. E. Banks, T. J. Davies, G. G. Wildgoose, R. G. Compton, *Chem. Commun.* (2005) 829.

CHAPTER 4

ELECTROCATALYTIC PROPERTIES OF IRON-PHTHALOCYANINE-SWCNT BASED ELECTRODES: THIOCYANATE AS A MODEL ANALYTE

4.1 Square wave voltammetric detection of SCN^-

Figure 4.1 shows a typical comparative square wave voltammetric (SWV) evolutions obtained at constant concentration (1 mM) of SCN^- at the various electrodes. The following deductions can be made from these voltammograms. First, it clearly shows that the current response at the various electrodes follows this trend: Au-Cys-SWCNT-FeOHETPc > Au-Cys-SWCNT-FeTAPc > Au-Cys-SWCNT > Au-Cys ≈ Au-FeOHETPc > Au-FeTAPc ≈ Bare Au (see figure 4.1 for abbreviations). The enhanced current response of the FeOHETPc and FeTAPc in the presence of the SWCNTs is a clear indication that the aligned SWCNTs enhance the electronic communication between FeOHETPc and FeTAPc and the bare gold electrode. It may be concluded here that it is the combined synergistic activities of these iron phthalocyanine (FePc) complexes (good catalysts) and the SWCNTs (efficient electronic conducting nanowires) that is responsible for the enhanced response of the Au-Cys-SWCNT-FeOHETPc and Au-Cys-SWCNT-FeTAPc towards the detection of the SCN^- species.

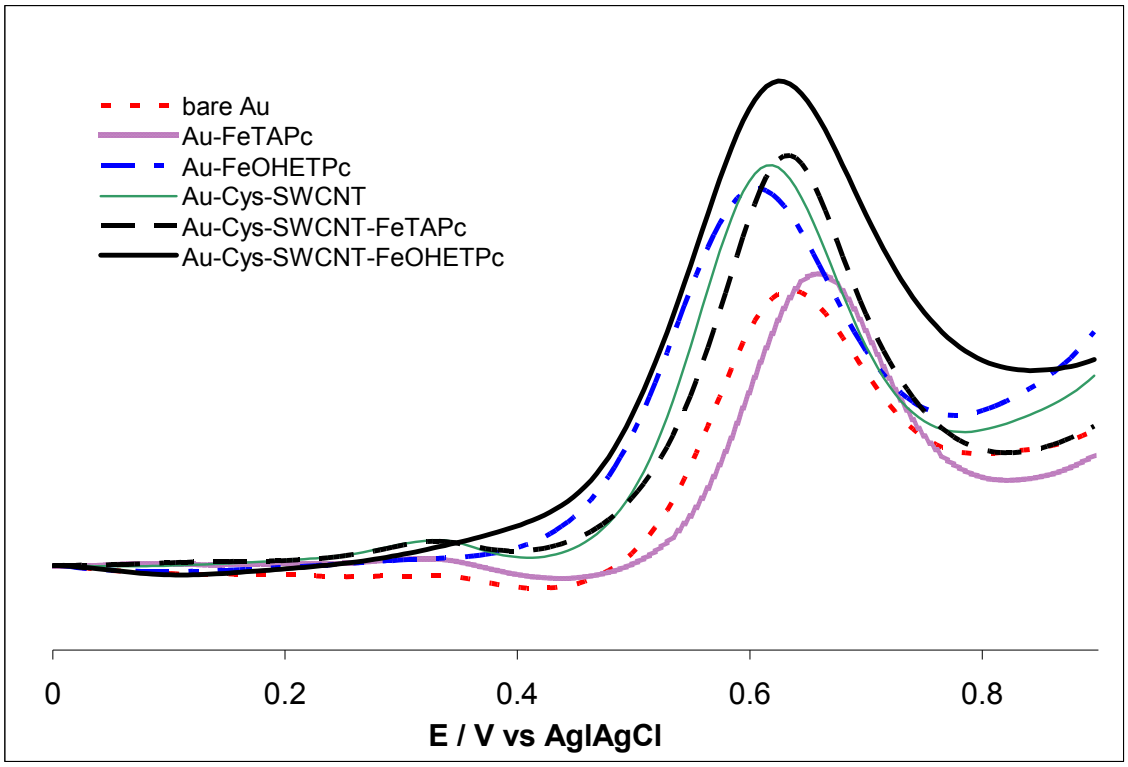

Figure 4.1: Typical comparative square wave voltammetric response of the various electrodes in PBS solution (pH 4.8) containing 1 mM SCN^-. Au-Cys voltammogram omitted for clarity.

Second, the weak peaks observed at the ~0.3 V for the electrodes modified with SWCNTs and the FePc complexes (FeOHETPc and FeTAPc) are attributed to the redox waves of the acidified SWCNT [1] and the $Fe^{(II)}/Fe^{(III)}$ [2], respectively. As it was recently observed [2], in acidic pH (0.5 M H_2SO_4) the Au-Cys-SWCNT shows pseudo-reversibility with anodic peak around 0.2 V (vs Ag|AgCl) and a cathodic peak at about –0.1 V (vs Ag|AgCl), thus the broadness of this peak for the Au-Cys-SWCNT-FeOHETPc electrode may be associated

with the overlap of both the redox waves of the SWCNTs and that of the FePc complexes.

Third, FeOHETPc-based electrodes gave better response than their FeTAPc counterparts. The electrocatalytic activity of the FeOHETPc-based electrodes started at less positive potentials and with greater current response compared to the FeTAPc-based electrodes. Of special note is the electrocatalytic activity of the Au-Cys-SWCNT-FeOHETPc that started from ~0.3 V compared to all the other electrodes that only started at ≥ 0.4 V. Some of the established factors that could influence the electrochemistry of MPc complexes are (i) the type of central metal ion; (ii) nature of axial ligands on the central metal; and (iii) the type and position of substituents (peripheral or non-peripheral, electron-donating or electron-accepting, and amount substituted from 1 to 16) at the macrocyclic phthalocyanine rings. Since the only structural difference between these two FePc complexes used in this work is the different substituent groups (-NH_2 and -SCH_2CH_2OH moieties), the high current response of the FeOHETPc over the FeTAPc is most likely to be due to the influence of these peripheral substituents. Thus, subsequent studies in this work, unless otherwise stated, were focused on the Au-Cys-SWCNT-FeOHETPc electrode.

4.2 Influence of scan rates on electrocatalysis of SCN^-

Cyclic voltammetric experiments were carried out with a view to establishing the impact of scan rates (ν) at constant concentration (1 mM) of the SCN^-. The study was carried out with both Au-Cys-SWCNT-FeOHETPc and Au-Cys-SWCNT-FeTAPc electrodes (exemplified in Figure 4.2(a) using Au-Cys-SWCNT-FeOHETPc). At both electrodes there were corresponding increases in the peak currents with increasing scan rates (scan rates ranging 25 - 1000 mV/s). Also, a broad reduction peak (in the 0.1 to 0.5 V regions) appearing only at higher scan rates, > 100 mVs^{-1}. A similar observation was reported in a previous study [3], where unsubstituted FePc was axially coordinated to the SAM of 4-mercaptopyrindine species on gold elelctrode (Au-4-MPyr-FePc) using the strategy introduced by Rubinstein and co-workers [4,5] (but only at > 25 mVs^{-1}), and was attributed to the reduction product(s) of the oxidised SCN^- species. The same explanation may hold for this study especially since it has been reported by others [6] that the oxidation of SCN^- is associated with several oxidation products via the unstable thiocyanogen $(SCN)_2$.

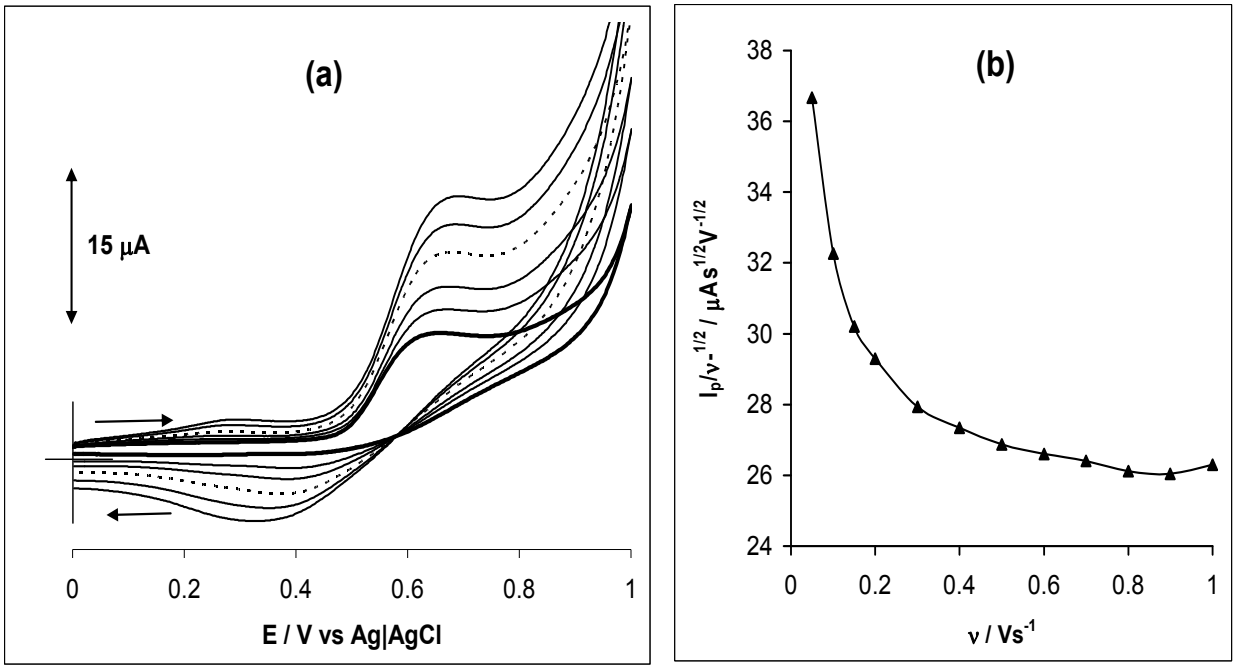

Figure 4.2: (a) Typical examples of cyclic voltammetric evolutions at varying scan rates (50, 150, 200, 400, 600 and 800 mVs^{-1}, inner to outer; outer omitted for clarity); and (b) Plot of current function ($I_p/\nu^{1/2}$) versus scan rate (ν) ranging from 50 to 1000 mVs^{-1}. [SCN^-] = 1 mM

The main reasons for the detection of these intermediate products of the oxidised SCN^- at > 25 mVs^{-1} for the Au-4-MPyr-FePc and at >100 mVs^{-1} for the Au-Cys-SWCNT-FeOHETPc are not apparent at this moment, but may be connected with the different reactivities of these two types of SAM-based electrodes. It could be interesting to further investigate this observation in future studies. The current function ($I_p/\nu^{1/2}$) decreased with the scan rate (figure 4.2b) which is

indicative of a coupled chemical reaction, EC_{cat} mechanism [7-9]. Peak current (I_p) of the SCN^- oxidation gave a linear relationship with the square root of scan rate ($\nu^{1/2}$) (R^2 = 0.9985), indicating a diffusion-controlled reaction. A plot of I_p vs ν was not linear proving that neither the oxidized SCN^- nor its intermediate product(s) adsorbed on the modified electrode.

The equation for an irreversible diffusion controlled process is given as Equation 4.1 [10]:

$$E_p = \frac{b}{2}\log\nu + \text{constant.} \qquad (4.1)$$

where b = Tafel slope = $0.059/\alpha n_\alpha$, α is the electron transfer coefficient, while $n\alpha$ is the number of electrons involved in the rate-determining step). The plots of the E_p vs $\log\nu$ gave linear equations as shown in equation 4.2.

$$E_p \text{ (V)} = (58.66\pm1.09)\text{x}10^{-3}\ log\,\nu + (787.60\pm 0.66)\text{x}10^{-3}$$
$$(R^2 = 0.9989) \qquad (4.2)$$

Assuming an electron transfer coefficient (α) $\approx$ 0.50, the values of the Tafel slope was *ca.* 117 $mVdecade^{-1}$, which is in excellent agreement with the ideal value of 118 $mVdecade^{-1}$ for a one-electron process in the rate-limiting step [11]. This value agrees with the report using

cobalt tetraethoxythiophenephthalocyanine as electrocatalyst [12]. Thus, this present result clearly suggests (i) the participation of a one-electron activity in the rate-determining step (rds) of the SCN^- oxidation at the Au-Cys-SWCNT-FeOHETPc, and (ii) that neither SCN^- nor its intermediate product(s) irreversibly adsorb on the electrode since such process should be expected to raise the Tafel slope to values higher than 120 mV/decade [11].

FePc complex is a mimic of the horse radish peroxidise (HRP), and according the work of Adak *et al* [6], HRP-catalysed oxidation of SCN^- occurs by two one-electron process with the intermediate formation of thiocyanate radicals. The radical readily dimerise to form the unstable thiocyanogen $(SCN)_2$. The $(SCN)_2$ is unstable in aqueous solution and readily hydrolyses to form some stable intermediate products. It is also well known that metalloporphyrin- and metallophthalocyanine-catalysed reactions of SCN^- usually occur by initial binding of the SCN^- to the central metal [13]. From these information and all the results (notably the involvement of the one electron process in the rate determining step as well as the coupled chemical reactions) obtained from the scan rate studies, the following reaction mechanism is suggested (Equations 4.3-4.8):

$$Fe^{(II)}OHETPc \longrightarrow Fe^{(III)}OHETPc + e- \quad (4.3)$$

$$Fe^{(III)}OHETPc + SCN^{-} \longrightarrow [SCN\text{-}Fe^{(III)}OHETPc]^{-} \text{ (axial ligation)} \quad (4.4)$$

$$[SCN\text{-}Fe^{(III)}OHETPc]^{-} \longrightarrow [SCN\text{-}Fe^{(III)}OHETPc] + e- \text{ (rds)} \quad (4.5)$$

$$[SCN\text{-}Fe^{(III)}OHETPc] \longrightarrow Fe^{(II)}OHETPc + {}^{\cdot}SCN \quad (4.6)$$

$${}^{\cdot}SCN + {}^{\cdot}SCN \longrightarrow (SCN)_2 \text{ (fast)} \quad (4.7)$$

$$(SCN)_2 + H_2O \longrightarrow \text{Reaction products} \quad (4.8)$$

The instability of the $(SCN)_2$ may partly be responsible for the inability to observe the reduction peaks at slow time scale, small scan rates. The onset of the electrocatalysis of SCN^- at the Au-Cys-SWCNT-FeOHETPc close to the redox wave of the Fe(II)/Fe(III) suggests the involvement of the central metal and axial ligation process in the catalysis.

4.3 Rotating gold disk electrode experiments

Further experiments were performed using rotating gold disk electrode (RDE) linear scan voltammetry technique. The RDE voltammetric evolutions of constant concentration (1 mM SCN^-) at different rotating speed of electrodes with their Koutecky-Levich plots is shown in Figure 4.3. The Koutečky-Levich plot (Figure 4.3 inset) was obtained from the conventional Koutecky-Levich theory [10], Equation 4.9:

$$\frac{1}{i_{\lim}} = \frac{1}{i_k} + \frac{1}{i_d} = \frac{1}{nFAkC} + \frac{1}{0.62nFACD^{2/3}\gamma^{-1/6}\omega^{1/2}} \qquad (4.9)$$

where $i_{\lim}$ is the measured current, i_k and i_d are the kinetic and diffusion-limited currents, respectively. C is the bulk concentration and γ is the kinematic viscosity of the solution which was estimated from 4 M SCN^- as 0.8145 cm s^{-1} [14]; other symbols retain their usual meanings. The numbers 1 to 10 in the figure correspond to 250 to 3000 $rads^{-1}$. The results showed that the catalytic current increased linearly with increasing $\omega^{-1/2}$ with a positive intercept, indicating that the electrode reactions were controlled by both kinetics at the electrode surface and the mass transport of SCN^- species at the

electrode surfaces. From the intercept and the slope of the plot, the diffusion coefficient value of *ca*. 1.30 x 10^{-5} cm^2s^{-1} was obtained.

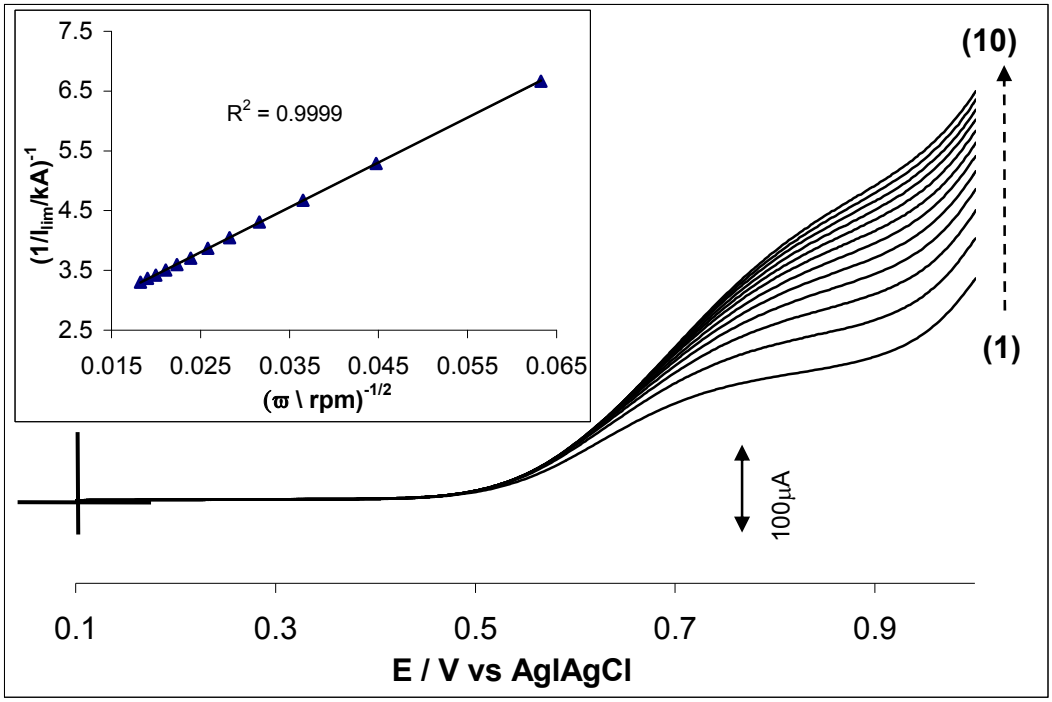

Figure 4.3: Linear sweep voltammetric evolutions of the rotating disk electrode experiments obtained at Au-Cys-SWCNT-FeOHETPc in PBS solution (pH 4.8) containing 1 mM SCN^- at 50 mVs^{-1}. (Inset is Koutečky-Levich plot.

About 28 years ago, Shimizu and Osteryoung had reported the oxidation of SCN^- at a rotating silver disk electrode (taking n = 1) and obtained a diffusion coefficient of (2.15±0.02) x10^{-5} cm^2s^{-1} [15]. If the

same one-electron process is assumed, the value for D is approximately 3.60 x 10^{-5} cm^2s^{-1}, which is the same magnitude as the their report [15], the slight difference which suggests that the diffusion of SCN^- is faster at Au-Cys-SWCNT-FeOHETPc than the bare gold electrode could be ascribed to differences in experimental conditions. Using the Koutecky-Levich equation, the k value was obtained *ca*. 1.40 x 10^{-2} cm^3 mol s^{-1}.

It should be mentioned here that the electrodes (Figures 4.1 – 4.3) were stable in the acidic and neutral pH conditions in the potential window of –0.5 and +1.0V vs Ag|AgCl, a similar behaviour to the thiol-derivatised MPc SAMs that we reported previously [3]. The reason for the stability exhibited by the Au-Cys-SWCNT-FeOHETPc electrode may be due to the protection of the underlying cysteamine sulphur by the aligned SWCNTs and macrocyclic ring of the phthalocyanine. However, I advise caution when using the electrode for electroanalysis not to go beyond the +1.0 V vs Ag|AgCl to avoid electro-oxidative desorption of the film.

4.4 Chronoamperometric investigations

Double potential step chronoamperometric experiments were recorded by polarizing the working electrode potentials to 0.62 and 0.20 V (Figure 4.4). Figure 4.4 shows a well resolved double-step chronoamperometric evolutions obtained at the Au-Cys-SWCNT-FeOHETPc electrode in the absence (buffer alone) and presence of consecutive addition of 32.3 μM thiocyanate in phosphate buffer solution (pH 4.8) (The numbers 1 to10 in figure 4.4, correspond to 0.0, 32.3, 62.5, 90.9, 118, 167, 211, 250, 302 and 333 μM, respectively.). It shows that at the conditions employed for this work, the SCN^- was irreversible. Figure.4.4 (inset) depicts linearity (R^2 = 0.9987) between log I_p versus log [SCN^-] with a slope (0.8818) close to unity, suggesting that one SCN^- species interacts with one molecule of the FeOHETPc complex. Also, a linear relation was obtained for the I_p vs [SCN^-] as in Equation 4.10:

$$I_p\,(A) = (4.20 \pm 0.09)\times10^{-3}\,[SCN^-]/M + (2.37 \pm 0.1)\times10^{-7} \quad (R^2 = 0.9964) \qquad (4.10)$$

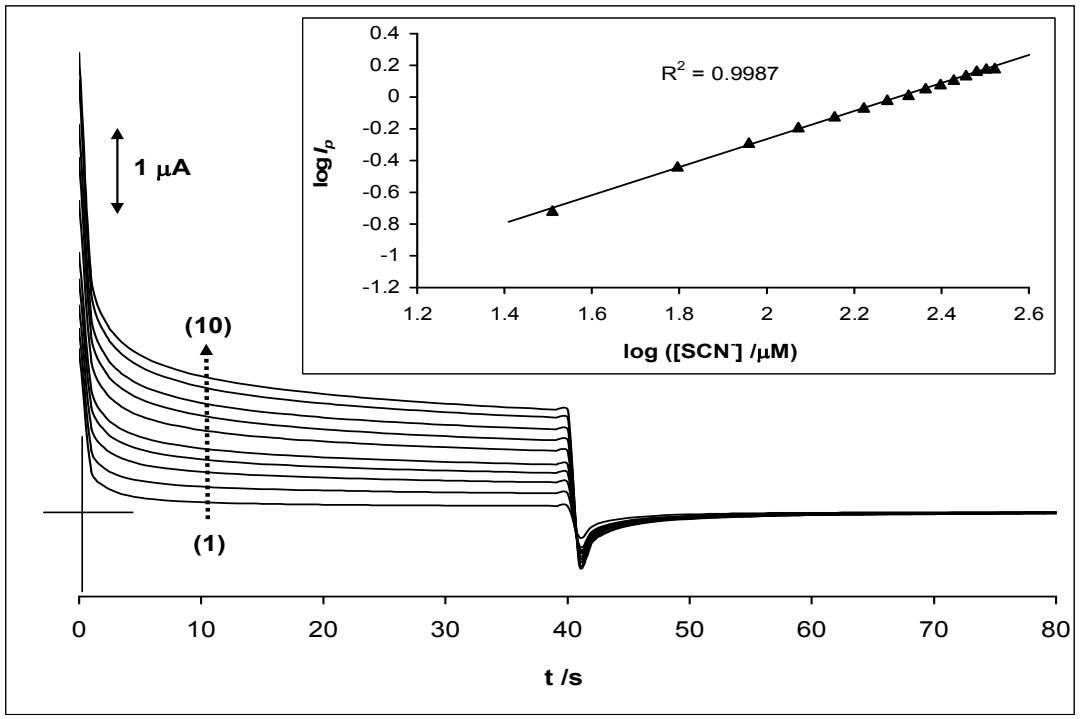

Figure 4.4: Typical double potential step chronoamperometric transients at Au-Cys-SWCNT-FeOHETPc in PBS solution (pH 4.8) following addition of SCN^- The potential was stepped from +0.62 to +0.20 and back to +0.62 V. Other chronoamperograms obtained during same experiments are omitted here for clarity purpose. Inset is the plot of chronoamperometric current at t = 10s vs log [SCN^-].

In the experimental conditions used in this work, a linear concentration range of up to 0.33 mM with a sensitivity of ca. $4.2x10^{-3}$ AM^{-1}, and limit of detection ~ 15 μM (LoD = 3.3 s/m [16], where s is the relative standard deviation of the intercept and m the slope of the linear peak current vs the concentration of SCN^-) were obtained

From the chronoamperometric data, both diffusion coefficient (D) and catalytic rate constant of SCN^- were also determined. For D, the Cottrell equation (Equation 4.11) was used:

$$I = \frac{nFAD^{1/2}C}{\pi^{1/2}t^{1/2}} \qquad (4.11)$$

where n is the number of electrons involved in the reaction, F is the Faraday constant (96485 C mol^{-1}), and A is the experimentally determined area of the electrode, C is the bulk concentration of the thiocyanate ($mol.L^{-1}$)), while t is time (s). It can be seen that the plots of $I_p \ vs \ t^{-1/2}$ at different thiocyanate concentrations is linear (Figure4.5), and from the plot of slopes vs [SCN^-], and taking n = 2, the D value for SCN^- was estimated to be *ca.* 7.70×10^{-6} cm^2s^{-1}, which is about 60% lower than that obtained at the RDE experiment.

The catalytic rate constant for the oxidation of SCN^- was also estimated from the chronoamperometry experiments using the relationship [17,18] (Equation 4.12):

$$\frac{I_{cat}}{I_{buff}} = \pi^{1/2}(kCt)^{1/2} \qquad (4.12)$$

where I_{cat} and I_{buff} are the currents in the presence and absence of thiocyanate, respectively; *k* is the catalytic rate constant and t is the time in seconds.

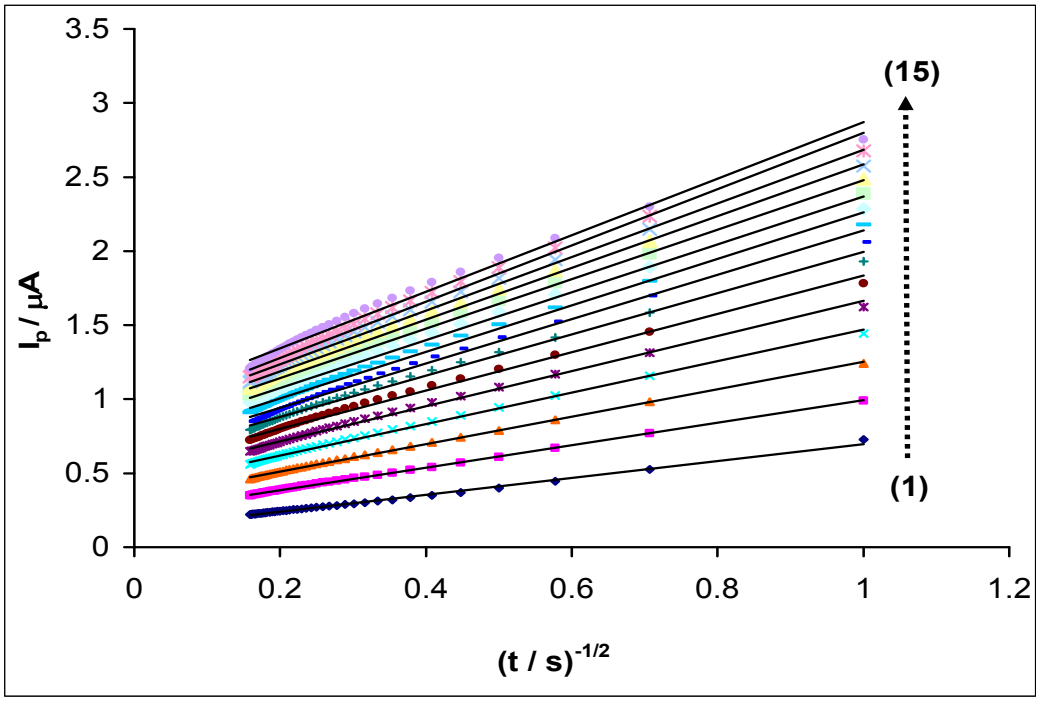

Figure 4.5: Typical Cottrell equation plots obtained from the chronoamperometric evolution at Au-Cys-SWCNT-FeOHETPc in PBS solution (pH 4.8) following addition of SCN^-. (The numbers 1 to15 correspond to 32.3, 62.5, 90.9, 118, 143, 167, 189, 211, 231, 250, 268, 286, 302, 318 and 333 µM, respectively)

From the plots of I_{cat}/I_{buff} vs $t^{1/2}$ at different thiocyanate concentrations (Figure 4.6), and a plot of the slopes vs $[SCN^-]$, k was estimated as 1.84×10^4 $cm^3 mols^{-1}$. Similar chronoamperometric experiments with Au-Cys-SWCNT-FeTAPc gave sensitivity, rate constant and diffusion coefficient as $2.90 \pm 0.04 \times 10^{-3}$ AM^{-1}, 0.82×10^4 cm^3 mol s^{-1} and 5.97×10^{-6} $cm^2 s^{-1}$, respectively. These data satisfactorily corroborate the SWV results shown in Figure 4.1.

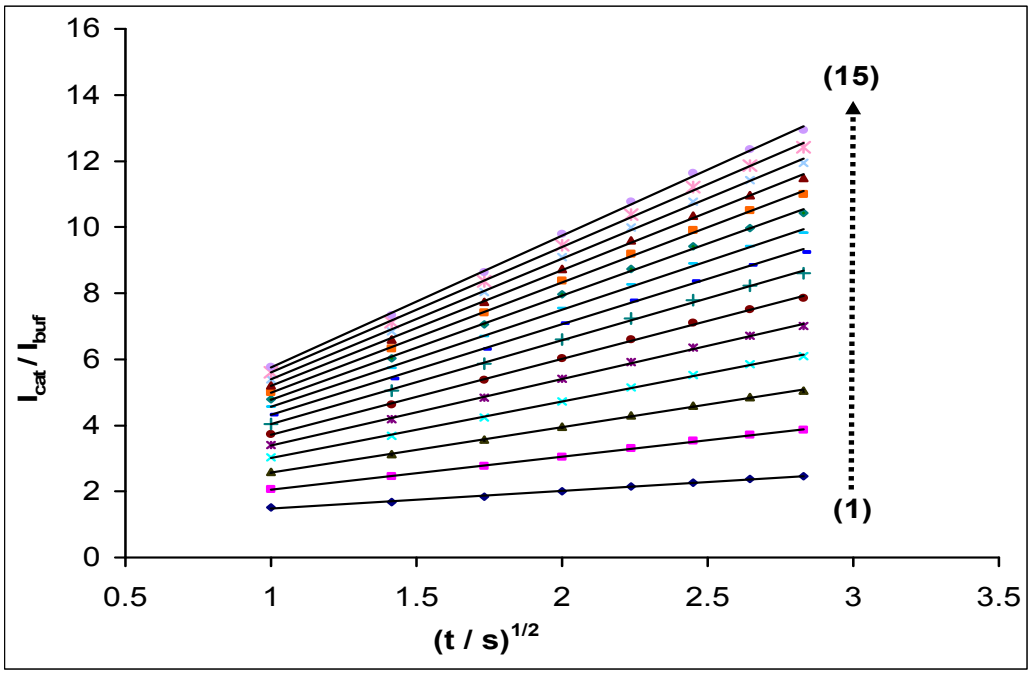

Figure 4.6: Plots of I_{cat}/I_{buff} vs $t^{1/2}$ obtained from the chronoamperometric evolution at Au-Cys-SWCNT-FeOHETPc in PBS solution (pH 4.8) following addition of SCN^-. (The numbers 1 to 15 correspond to 32.3, 62.5, 90.9, 118, 143, 167, 189, 211, 231, 250, 268, 286, 302, 318 and 333 μM, respectively)

4.5 Real sample analysis with smoker's saliva

Saliva is produced by the salivary glands and human saliva is 98% water but contains many important substances including electrolytes, mucus and antibacterial compounds and various enzymes. One of the the antibacterial compound is thiocyanate, hydrogen peroxide and secretory immunoglobulin A [19]. This study has proved that the amount of thiocyanate in human saliva of a non smoker is minimal.

For a check on the suitability of the Au-cys-SWCNT-FeOHETPc electrode for possible application as a biological sensor, the electrode was used for a comparative chronoamperometric determination of SCN^- in saliva samples of smoker and non-smoker. Figure 7.1 is an example of a typical comparative chronoamperograms in buffer solution, and buffer solutions containing saliva samples of a smoker and a non-smoker. It is clearly seen that current response to the non-smoker saliva sample is approximately as the buffer solution while that of the smoker is well pronounced. The SCN^- concentration in the saliva samples of the smoker was estimated as 38.6±0.76 μM while that of the non-smoker was 4.56±4.02 μM (n = 5).

The ability of this electrode to clearly discriminate between a smoker and non-smoker suggests that it could possibly be applied for such biological analysis in clinics.

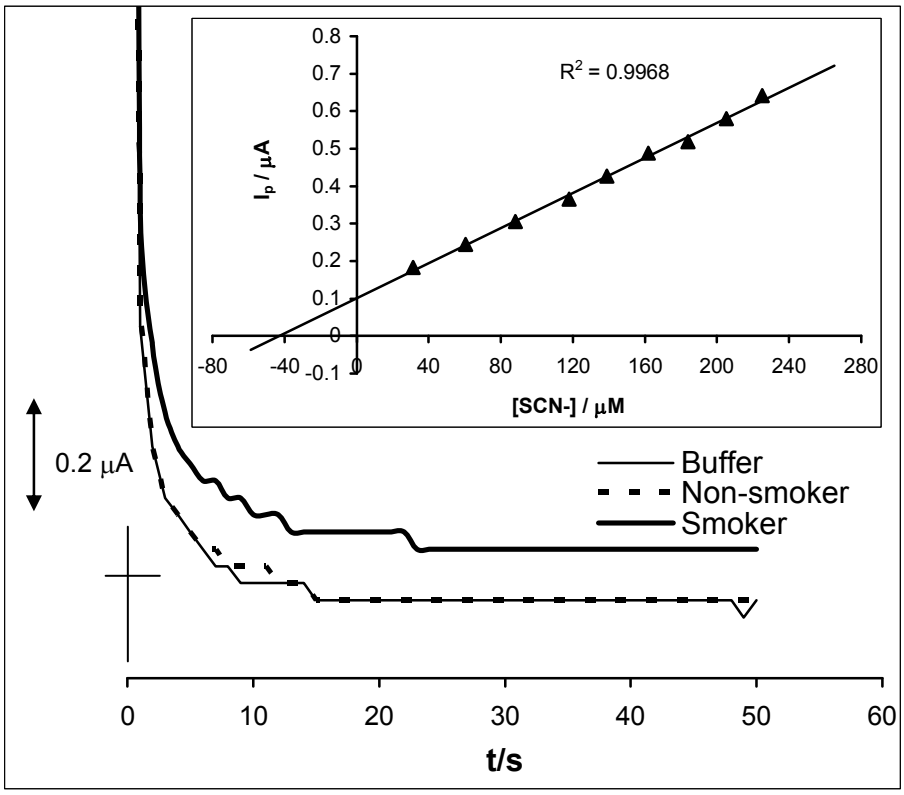

Figure 4.7: Typical example of chronoamperometric response of the saliva samples of a smoker and a non-smoker at the Au-Cys-SWCNT-FeOHETPc electrode in PBS solution (pH 4.8), fixed potential = 0.62 V vs Ag|AgCl. Inset is an example of one the replicate results of the standard addition methods.

REFERENCES

1. H. Luo, Z. Shi, N. Li, Z. Gu, Q. Zhuang, *Anal. Chem.* 73 (2001) 915.
2. K. I. Ozoemena, T. Nyokong, P. Westbroek, *Electroanalysis* 15 (2003) 1762.
3. K. I. Ozoemena, T. Nyokong, *J. Electroanal. Chem.* 579 (2005) 283.
4. G. Kalyuzhny, A. Vaskevich, G. Ashkenasy, A. Shanzer, I Rubinstein, *J. Phys. Chem. B.* 104 (2000) 8238.
5. Ashkenasy, G. Kalyuzhny, J. Libman, I Rubinstein, A. Shanzer, *Angew. Chem. Int. Ed. Engl.* 38 (1999) 1257.
6. S. Adak, A. Mazumdar, R. K. Banerjee, *J. Biol. Chem.* 272 (1997) 11049.
7. P. M. S Monk, Fundamentals of Electroanalytical Chemistry, John Wiley and Sons, Chichester, 2001, p.172
8. L. Nadjo, J. M. Saveant, *J. Electroanal. Chem.* 48 (1970) 113.
9. R. S. Nicholson, I. Shain, *Anal. Chem.* 36 (1994) 706.
10. A. J. Bard and Faulkner, Electrochemical Methods: Fundamentals and applications, 2nd ed., John Willey & Sons, Hoboken, NJ., 2001.
11. J. A. Harrison, Z. A. Khan, *J. Electroanal. Chem.* 28 (1970) 131.
12. N. Sehlotho, T. Nyokong, *Electrochim. Acta* 51 (2006) 4463.

13. K. I. Ozoemena, T. Nyokong, In Encyclopedia of Sensors, C. A Grimes, E.C. Dickey, M.V. Pishko, Eds., American Scientific Publishers, California, 3 (2006) Chapter E, pp.157.

14. A. V. Balmasov, E. V. Koroleva, S. A. Lilin., *Protect. Met.* 41 (2005) 35.

15. K. Shimizu, R. A. Osteryoung, *Anal. Chem.* 53 (1981) 2351

16. G. D. Christian, Analytical Chemistry, 6th ed. John Wiley and Sons, New York, 2004, p.113.

17. M. H. Pournaghi-Azar, R. Sabzi, *J. Electroanal. Chem.* 543 (2003) 115.

18. K. M. Manesh, P. Santosh, A. I. Gopalan, K. -P. Lee, *Electroanalysis* 18 (2006) 894.

19. M. Anthea, J. Hopkins, C. W. McLaughlin, S. Johnson, M. Q. Warner, D. LaHart, J. D. Wright, *Human Biology and Health*. Englewood Cliffs, New Jersey, USA: Prentice Hall (1993),

CHAPTER 5

MICROSCOPIC AND ELECTROCHEMICAL PROPERTIES OF FERROCENE SINGLE-WALLED CARBON NANOTUBES BASED ELECTRODES

5.1 SAM formation strategies

Monolayers of alkanethiol capped with carboxylated ferrocene and single-walled carbon nanotubes were prepared by self-assembly technique on gold surfaces. Scheme 5.1 and 5.2 summarizes the self-assembly technique which employed the normal carbodiimide coupling chemistry [1] whereby the –COOH functional groups are first activated to permit the covalent bonding with the $-NH_2$ groups of the cysteamine. The gold electrode modified with cysteamine is represented as Au-Cys. The formation of Au-Cys-FDCA and Au-Cys-FMCA followed after placing the Au-Cys electrode in a 1 ml DMF solution containing 0.5 mg (*ca.* 2μmol) of DCC and 1 mg (*ca.* 4 μmol) of FDCA or 1mg (*ca.* 4μmol) FMCA for 48hr, respectively. The Au-Cys-SWCNT-FDCA electrode was obtained by placing Au-Cys in 1ml DMF solution containing a mixture of SWCNT (1 mg) and FDCA (1 mg) and 0.5 mg DCC for 48hr. This same method was used to prepare Au-Cys-SWCNT-FMCA. Upon removal from the deposition solution, prior to electrochemical experiments, the electrode was thoroughly rinsed with millipore water and dried in a nitrogen atmosphere. The modified electrode was conditioned by placing in 0.5 M H_2SO_4 and repetitively scanned between −0.5 and 0.6 V (vs Ag|AgCl) potential window at a scan rate of 25 mVs^{-1} until a constant scan was obtained.

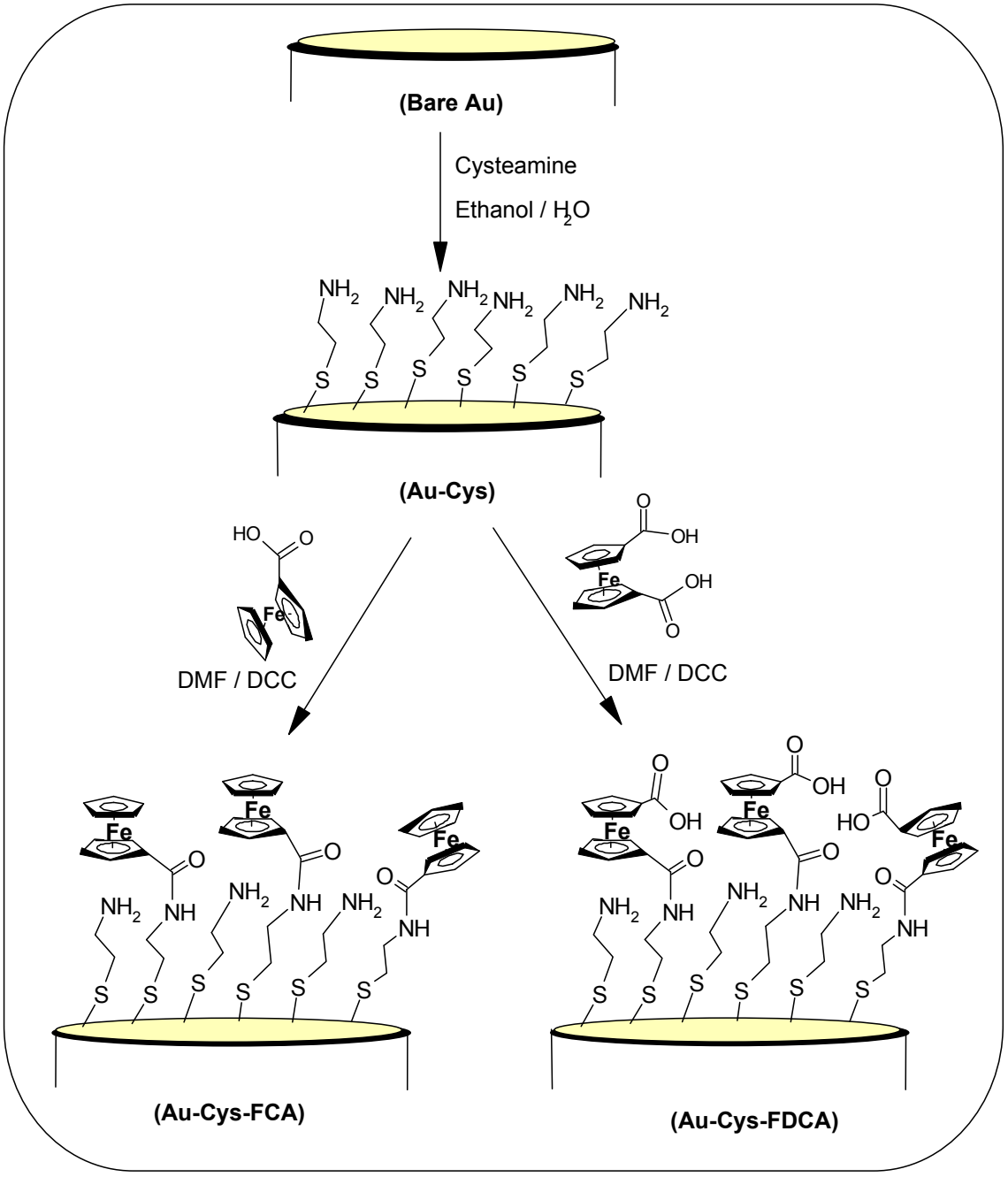

Scheme 5.1: Schematic of the gold electrode modification routes for Au-Cys, Au-Cys-FCA and Au-Cys-FDCA.

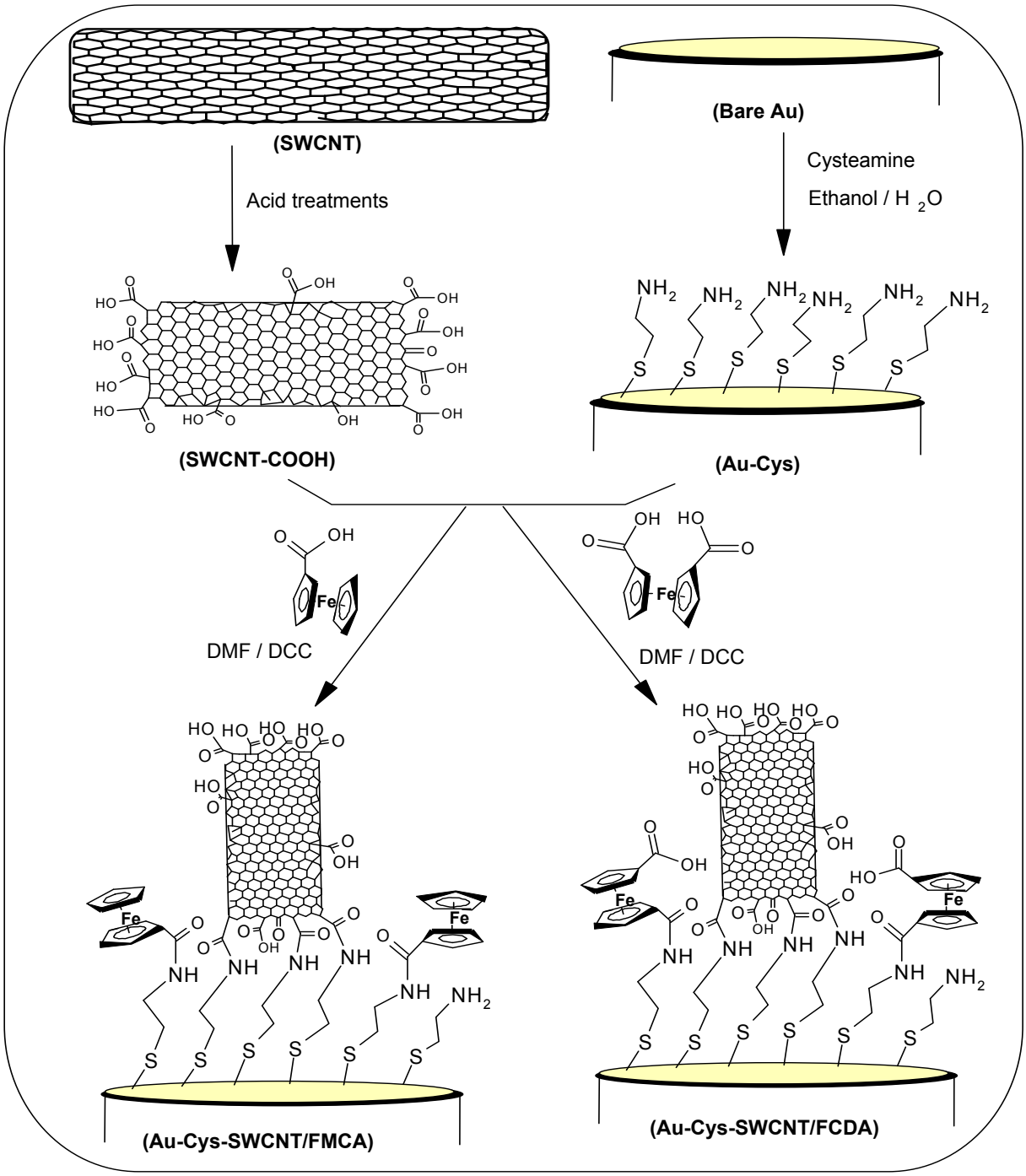

Scheme 5.2: Schematic of the gold electrode modification routes for Au-Cys-SWCNT/FMCA and Au-Cys-SWCNT/FDCA.

5.2 Atomic force microscopic characterization

Figure 5.1 summarizes the fabrication sequences for self-assembling of the SWCNTs, FCDA and FMCA onto gold electrode. Confirmation of the attachment of these redox-active species, by self-assembly technique was achieved by the use of atomic force microscopy. Figure 5.1 compares the AFM images of (a) bare Au, (b) Au-Cys-SWCNT, (c) Au-Cys-FDCA and (d) Au-Cys-SWCNT/FDCA. The needle-like protrusion of the Au-Cys-SWCNT agrees with several reports for SWCNT-based SAMs [2,3]. Typical lengths of acid-treated SWCNTs using the conditions used in this work lie in the 250 – 350 nm [4]. However, when we immobilized them as SAMs, the heights lie in the 30 – 50 nm range, which is in close agreement with literature [2]. The SWCNTs assembled as bundles and not as individual due to the strong van der Waal's attractive forces existing between carbon nanotubes. The same explanation may be true for the needle-like protrusion shown by the Au-Cys-FDCA. Interestingly, as would be expected, the mixed layers, Au-Cys-SWCNT/FDCA, showed more compactness than either the individual layers. Generally, the AFM topographic height and roughness in Figure 5.1 are greater with the combined SWCNT and Fc assemblies, exemplified with Au-Cys-SWCNT/FDCA (d). The rougness and height of the Au-Cys-SWCNT (b) are higher than those of the Au-Cys-FDCA (c) or Au-Cys-FMCA (not

shown), confirming that SWCNTs are longer than the FC assemblies (as indicated in the cartoon of scheme 5.2).

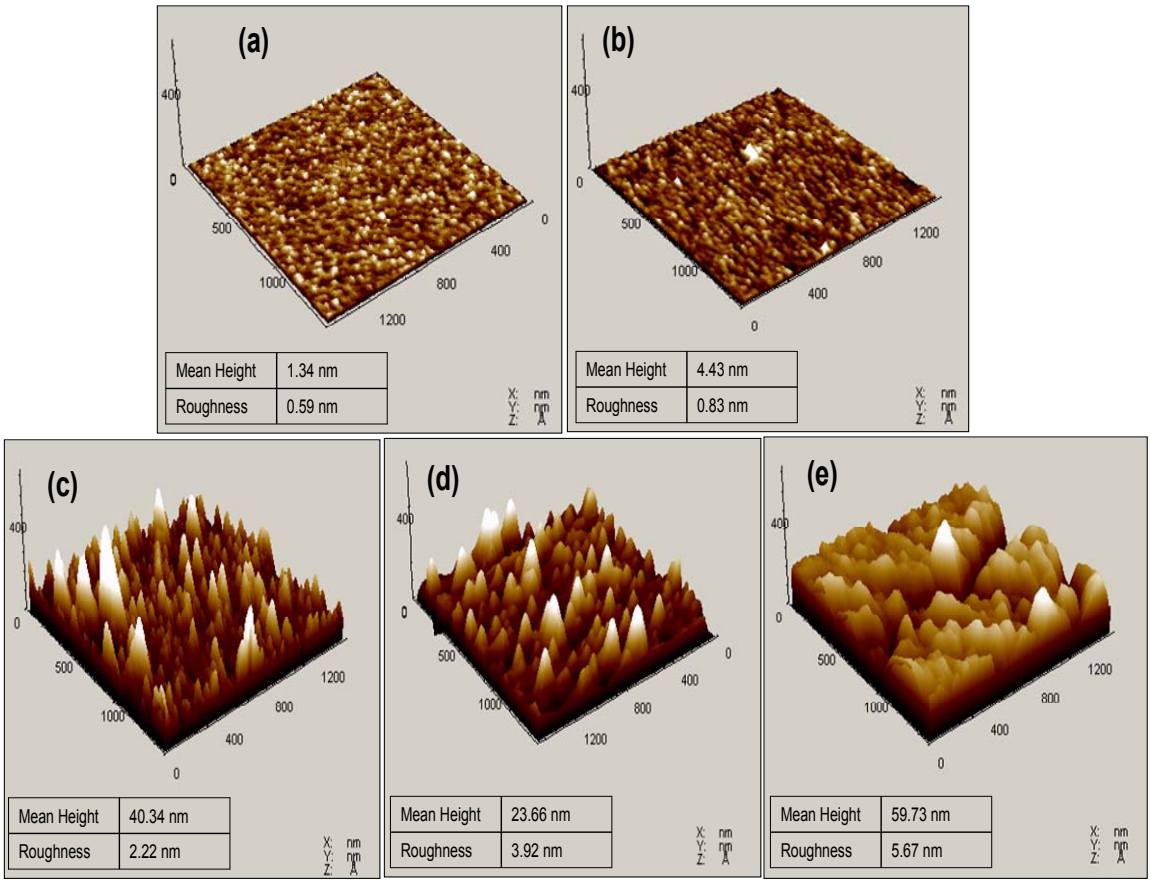

Figure 5.1: Topographic images of the electrodes: (a) Au bare, (b) Au-Cys, (c) Au-Cys-SWCNT, (d) Au-Cys-FDCA and (e) Au-Cys-SWCNT/FDCA.

5.3 Electron transfer dynamics in 0.5 M H_2SO_4 solution.

5.3.1 Cyclic voltammetric characterization

The cyclic voltammetric properties of the ferrocene-modified gold electrodes were studied in 0.5 M H_2SO_4 solution. Figure 5.2 shows the CV profiles of the electrodes obtained at 25 mVs^{-1}.

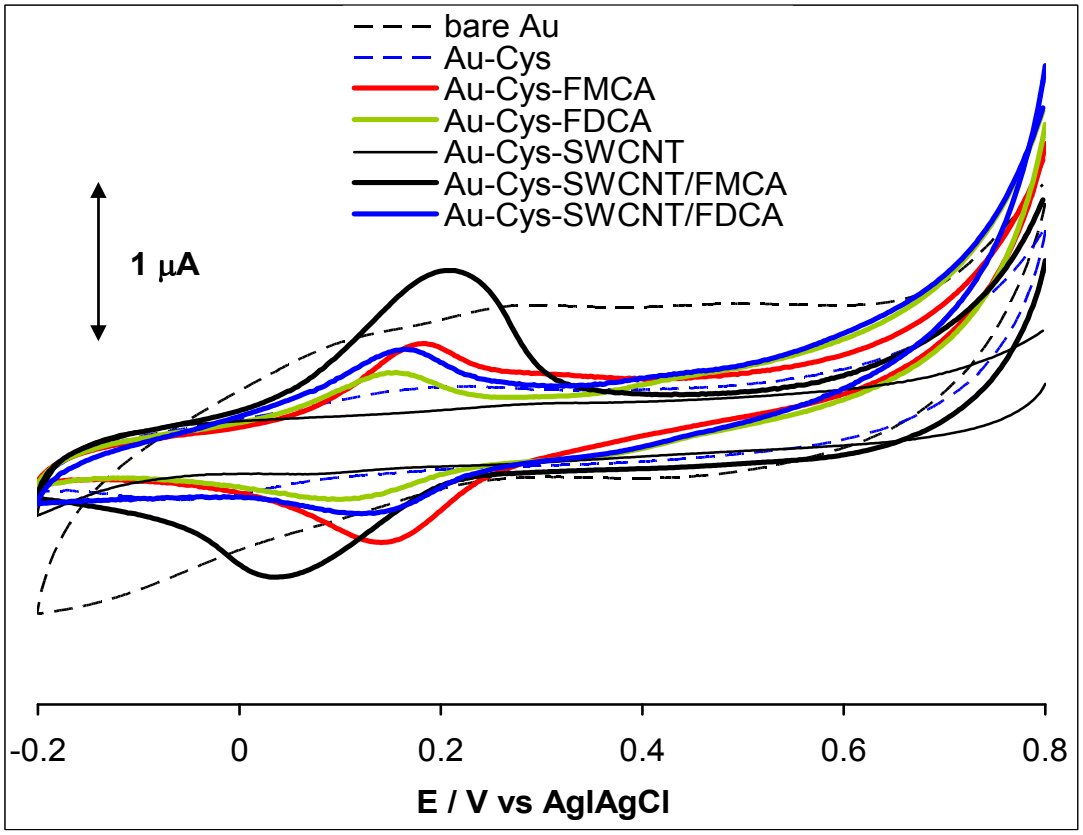

Figure 5.2: Comparative cyclic voltammetric evolutions of the modified gold electrode in 0.5 M H_2SO_4, Au-Cys-FCA, Au-Cys-FDCA, Au-Cys-SWCNT, Au-Cys-SWCNT/FMCA and Au-Cys-SWCNT/FDCA.

Each of the redox couples is ascribed to the Fe(III)/Fe(II) redox process. The electrochemical parameters, formal potential ($E_{1/2}$ / mV), peak-to-peak potential separation (ΔE_p / mV), the width at half the peak current (E_{fwhm} / mV) and ratio of anodic peak current to the cathodic peak (I_{pa}/I_{pc}) and surface coverages (Γ/molecule.cm^{-2}) are summarized in Table 5.1. All the electrodes show $I_{pa}/I_{pc} \approx 1$, indicating voltammetric reversibility. The choice of the potential used here was based on our experience working with thiolated SAMs. As we cautioned in previous reports on SAMs [5,6], the thiol monolayer only show remarkable stability in acidic and slightly alkaline pH (pH 2 – 9) at potential between window of –0.5 and +0.9 V vs Ag/AgCl. At more positive potential (≥ +0.9 V vs Ag|AgCl) thiol desorption and / or Au surface oxidation could be observed. The stability observed for these SAMs may be related to some extent by hydrogen bonds arising from the –COOH and –OH funtional groups. It may also be related to the protection of the sulfur by the large SWCNTs and and/or FC rings. The interchain attractive interactions resulting from the alkyl chains may also be another contributing factor.

As seen from Table 5.1, the electron transport (signified by the magnitude ΔE_p) in this acid electrolyte condition is fastest at the Au-Cys-SWCNT/FDCA ≈ Au-Cys-FMCA and slowest at the Au-Cys-SWCNT/FMCA. In a similar manner, the E_{fwhm} values (in the 71 – 117

mV range) slightly deviate from the ideal value of 90.6/n mV for n = 1 [7-9], with the Au-Cys-SWCNT/FMCA (117 mV) being slightly greater than that of the Au-Cys-SWCNT/FDCA (104 mV). The higher values of ΔE_p and E_{fwhm} for the SWCNT/FMCA compared to its SWCNT/FDCA counterpart may be related to different factors. First, some workers [3,4,10,11] have attributed such phenomenon to ferrocene species being located in a range of environments with a range of $E_{1/2}$. This should not be totally surprising considering the distribution of lengths of the SWCNTs on the gold substrate, and that the ferrocenes studied in this work could possibly be attached to the ends and/or defect sites of the SWCNTs via ester bonds (i.e., between the –COOH of the ferrocene and few –OH groups on the SWCNTs).

By different environments, it is meant that the ferrocene species have different formal potentials, and thus the effective voltammetric wave will consist of a superposition of distinct electrochemical responses, resulting in the observed voltammetric broadening [4]. It is worth pointing out that the formal redox potentials of the two FC species will be different. Also, as can be clearly seen from the the CVs, especially in the 0.3 – 0.8 V region, the backgroung current or capacitance of the bare Au (CAu) is about three times higher than the capacitance of any of the SAM-modified gold electrode (CAu-SAM).

Table 5.1: Summary of estimated voltammetric data obtained in 0.5 M H_2SO_4 (n = 4)

	Electrochemical parameters					
Electrodes	$E_{1/2}$ / mV	ΔE_p/ mV	E_{fwhm} / mV	I_{pa}/I_{pc}	$10^9\ \Gamma_a$/mol cm^{-2}	Γ_a/Γ_c
Au-Cys-FMCA	158	4.8	71	0.8	1.6±0.3	0.704
Au-Cys-FDCA	131	14.7	104	0.9	1.1±0.2	0.781
Au-Cys-SWCNT/FMCA	137	95.2	117	1.1	3.3±0.8	1.030
Au-Cys-SWCNT/FDCA	146	4.7	107	1.1	1.4±0.3	0.845

This is expected since as in aqueous solution, unlike in organic solutions, the overall electrode double-layer capacitance should be governed by the bare Au (i.e., CAu > CAu-SAM) [12,13].

The second explanation for the non-ideal ΔE_p and E_{fwhm} values for the adsorbed ferrocenes may be found from the works of Chidsey and co-workers [14-16]. According to these workers, when the self-assembled ferrocene species are well separated and do not interact with one another, a narrow symmetric redox peak with ideal E_{fwhm} value of 90.6/n mV will be obtained. However, as the concentration n of the ferrocene adsorbates increases, the resulting voltammograms will become asymmetric, broaden, with an increase in the ΔE_p value.

5.3.1.1 Surface coverage

The surface coverages were established from the CV profiles in 0.5M H_2SO_4 using the relationship:

$$\Gamma_{SAM} = \frac{Q}{nFA} = \frac{\int Idt}{nFA} \qquad (5.1)$$

where Q is the background-corrected charge under the cathodic or anodic waves, n = number of electrons involved in the redox process, F is the Faraday constant, and A is the area of the electrode. The surface coverage values are listed in Table 5.1. The average coverage increases as SWCNT/FMCA (3.3 x 10^{-9} mol cm^{-2}, 2.0 x 10^{15}

molecules/cm^{-2}) > Cys-FMCA (1.6 x 10^{-9} mol cm^{-2}, 9.6 x 10^{14} molecules/cm^{-2}) > SWCNT/FCDA (1.4 x 10^{-9} mol cm^{-2}, 8.4 x 10^{14} molecules/cm^{-2}) > Cys-FCDA (1.1 x 10^{-9} mol cm^{-2}, 6.6 x 10^{14} molecules/cm^{-2}). Since the maximum coverage expected of a monolayer of ferrocene is 4.5 x 10^{-10} mol cm^{-2} [4] (*ca* 2.7 x 10^{14} molecules cm^{-2} or ≈ 37 Å^2 per molecule), it means that the coverages obtained in this work are between 3 and 8 times higher than expected. It should however be noted that other workers have observed similar or even higher values compared to our results. For example, Gooding *et al*. [4] observed a much higher surface coverage (1.8±0.9 x 10^{-8} mol cm^{-2}) for randomly-distributed ferrocenes on SWCNTs and attributed this to the existence of a three-dimensional network of redox sites. Flavel *et al*. [10] observed a 1.14 x 10^{-9} mol cm^{-2} and 9.59 x 10^{-8} mol cm^{-2}) for macro- and nanoscale ferrocenemethanol-modified carbon nanotube electrodes on silicon, respectively. Chambers *et al*. [17] reported values of ~4 x 10^{14} molecules cm^{-2}. It is possible that the high surface coverages obtained in this work could be due to the long exposure time of cysteamine to gold electrode leading to more binding sites for the ferrocenes. The high surface coverage for the SWCNT/FMCA compared to SWCNT/FDCA suggests that FMCA species probably coordinate more with SWCNTs via ester bonds as described above compared to its FDCA counterparts. It is known from Chidsey

and co-workers [14-16] that high concentration of ferrocene adsorbates leads to asymmetric and broad voltammograms, hence high ΔE_p values.

Thus, the higher surface coverage shown by the FMCA-based electrode (Table 5.1) may further explain the poor ΔE_p and E_{fwhm} values of the SWCNT/FMCA compared to its SWCNT/FDCA counterpart.

5.3.1.2 Repetitive scanning

The voltammetric behaviour of the electrodes when subjected to repetitive scanning in acidic electrolyte was also investigated. This experiment is necessary for establishing the electrochemical stability of these redox-active adsorbates. Figure 5.5 shows typical voltammograms (1st and 20th scans of each electrode) obtained on repetitively scanning each electrode in the 0.5 M H_2SO_4 solution. For all the electrodes, we observed that the first few scans (*ca.* 1 – 5 scans) remained unchanged. However, as the scan number was increased, the voltammograms became broadened (thereby increasing both the E_{fwhm} and ΔE_p values) stabilising at about the 20th scan.

Unlike the low values of the ΔE_p seen at the first five scans (Table 5.1), at the 20th scan, the ΔE_p values increased to ~ 100 mV for the Cys-FMCA, > 200 mV for the Cys-FDCA, and ~100 mV for the SWCNT/FDCA. For the SWCNT/FMCA, however, there was a slight

decrease from its original 95 mV to about 80 mV at the 20th scan. This is an interesting observation considering that such behaviour has only been observed when the concentration of ferrocene adsorbates is increased [14-16]. Besides, Finklea [18] had demonstrated that the cause of such behavior arising from increase in concentration of the ferrocene to be due to double-layer effects arising from a rapid increase in surface charge during oxidation.

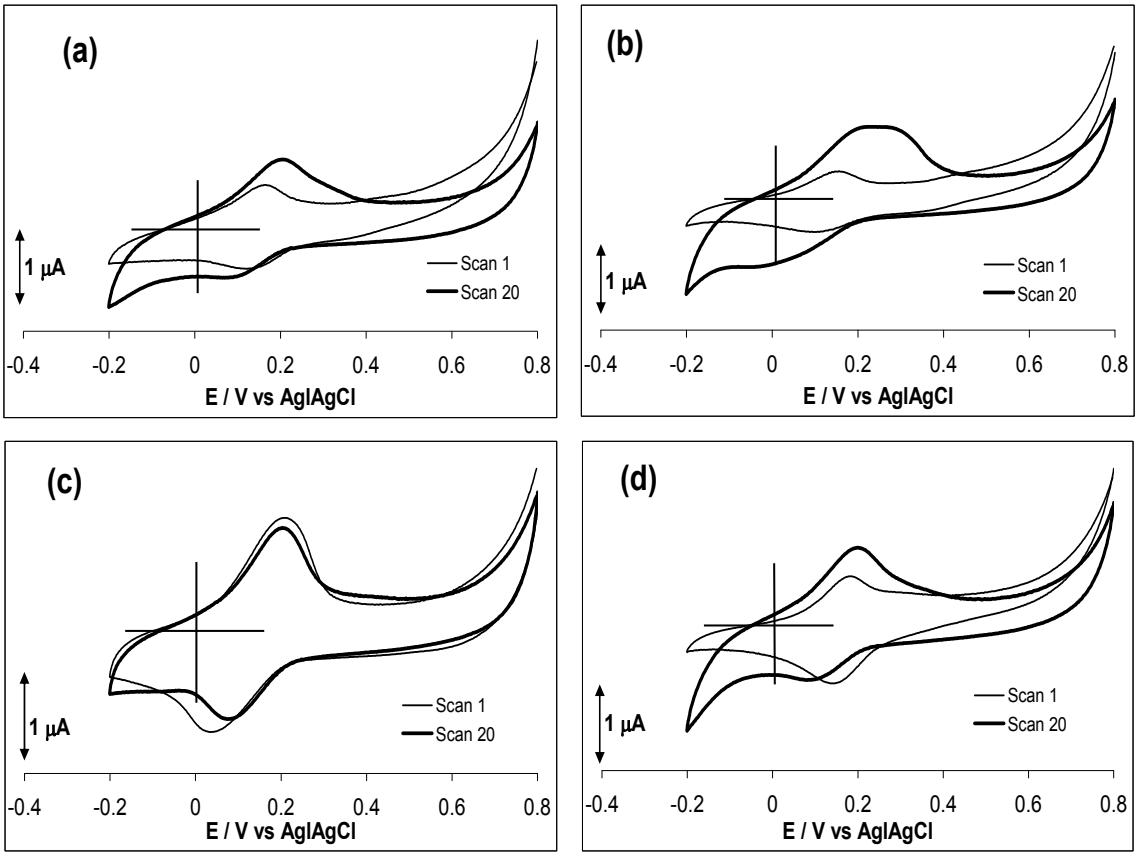

Figure 5.3: Comparative cyclic voltammetric evolutions of the modified gold electrode in 0.5M H_2SO_4 obtained at the 1st and the 20th scans for (a) Au-Cys-SWCNT/FDCA, (b) Au-Cys-FDCA, (c) Au-Cys-SWCNT/FMCA and (d) Au-Cys-FMCA. Scan rate = 25 mVs^{-1}.

In other words, surface charge effectively decreases the potential difference between the remaining unoxidised ferrocenes and the surface, and thus requiring a high applied bias for the oxidation of these ferrocene. But, in our case, since the concentration of the ferrocene species in each electrode is the same at all scans, the assumption of the asymmetric and broadening nature of the redox peaks during repetitive scanning may probably be due to the disordering of the initial well-separated ferrocene species to a form where they now interact with one another. Simply put, during the first few scans of the ferrocene-based electrodes, the ferrocenes head groups are still well-separated and do not interact with one another (indicated by the near-ideal E_{fwhm} value, Table 5.1). However, as the scanning number is increased, these ferrocenes may now begin to interact with one another and / or the double layer effects ensure. Also, it is worthy to note from Figure 5.5 that without the SWCNTs, the ΔE_p value is higher compared to when Ferrocene is co-assembled with the SWCNTs, suggesting that SWCNTs tend to suppress this double-layer effects (for example, compare the CVs of Au-Cys-FMCA and Au-Cys-SWCNT/FMCA).

The existence of the ferrocene redox activity during the repetitive scanning indicates that the modified electrodes exhibited strong electrochemical stability in 0.5 M H_2SO_4 solution. Such stability

is important for their electrochemical studies as well as their potential applications in acidic pH conditions. Thus, all subsequent experiment with each of the ferrocene-based electrode was performed after 20 continuous scanning in 0.5 M H_2SO_4 solution

5.3.2 Electrochemical impedimetric characterization

Electrochemical impedance spectroscopy (EIS) is an important technique for probing heterogeneous electron transfer (HET) kinetics, especially at gold electrode modified with self-assembled mono or multi-layers of redox-active or redox silent species [13,19-22]. To establish the HET kinetics in this acidic solution, EIS experiments were carried out for each of the modified electrode, as described by Creager and Wooster [19]. Figure 5.3(a) presents typical comparative Nyquist plots obtained for the four modified electrodes, biased at their approximate formal potential (~0.14 V vs Ag|AgCl). Interestingly, the experimental data were satisfactorily fitted with the modified Randles electrical equivalent circuit (Figure 5.3(b)), popularly used for modelling a redox-active monolayer on an electrode surface [13,19]. In the model, the R_s is the solution or electrolyte resistance, R_{ct} represents the electron-transfer resistance, while the true double layer capacitance (C_{dl}) is replaced by a constant phase element (CPE_1) and

Warburg impedance (Z_w) replaced by another constant phase element (CPE_2 or capacitance of the adsorbed molecules). The electron transfer rate constant (k_{et}) of each of the electrodes was obtained from: [13,19]

$$k_{et} = \frac{1}{(2R_{ct}CPE_2)} \qquad (5.2)$$

From Table 5.2, the k_{et} value increased as follows: Au-Cys-FMCA (~ 12 s^{-1}) ≈ Au-Cys-SWCNT/FDCA (~ 10 s^{-1}) > Au-Cys-FDCA (~ 0.8 s^{-1}) > Au-Cys-SWCNT/FMCA (~ 0.3 s^{-1}), in close agreement with of the CV data listed in Table 5.1.

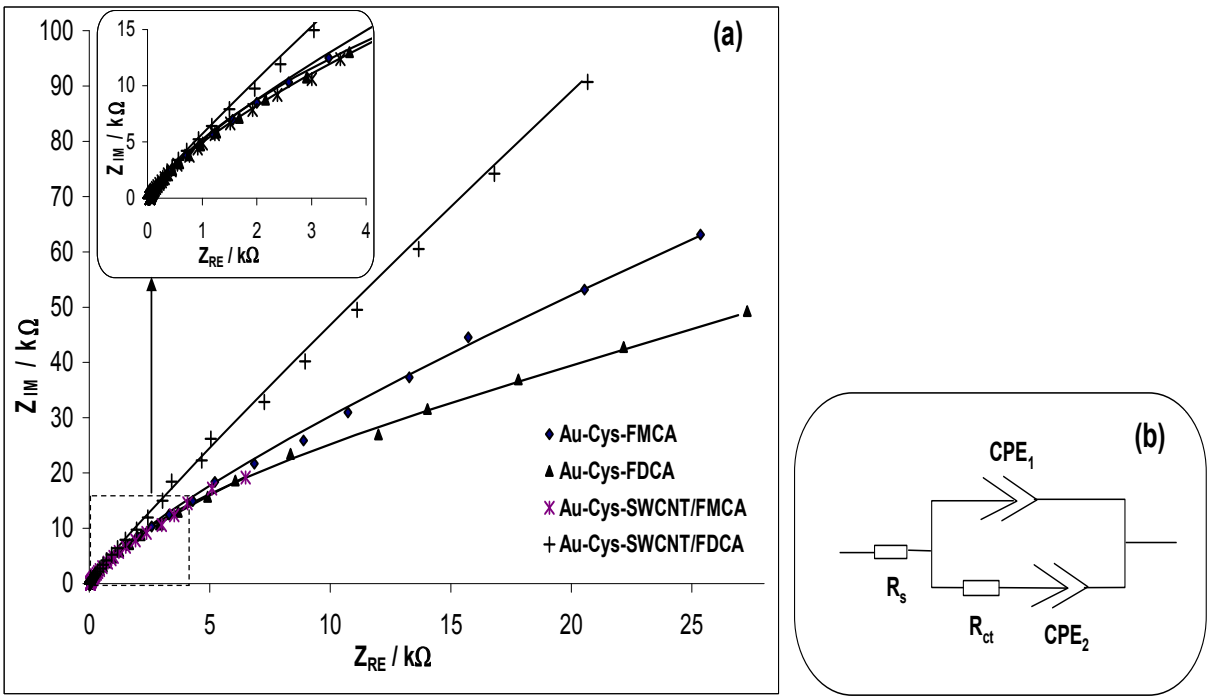

Figure 5.4 Nyquist plots (a) of the modified electrodes in the H_2SO_4 solution and (b) Equivalent circuit used in fitting (a).

It is interesting to observe how the neighbouring SWCNTs impact on the HET of the two different types of ferrocenes, SWCNTs improve the HET of ferrocene with exposed –COOH groups (FDCA) but decrease the HET of the ferrocene containing no pendant –COOH groups (FMCA).

The impedance of a CPE (Z_{CPE}) is defined as [23,24]:

$$Z_{CPE} = \frac{1}{[Q(j\omega)^n]} \qquad (5.3)$$

where Q is the frequency-independent constant relating to the surface electroactive properties, ω is the radial frequency, the exponent n arises from the slope of log Z vs log f (and has values $-1 \leq n \leq 1$). If $n = 0$, the CPE behaves as a pure resistor; $n = 1$, CPE behaves as a pure capacitor, $n = -1$ CPE behaves as an inductor; while $n = 0.5$ corresponds to Warburg impedance (Z_w) which is associated with the domain of mass transport control arising from the diffusion of ions to and from the electrode|solution interface. In general terms, CPE arises from such factors as (i) the nature of the electrode (e.g., roughness and polycrystallinity), (ii) distribution of the relaxation times due to heterogeneities existing at the electrode/electrolyte interface, (iii) porosity and (iv) dynamic disorder associated with diffusion [25].

Table 5.2: Summary of estimated EIS parameters obtained in 0.5 M H_2SO_4

Electrodes	Electrochemical Impedemetric parameters[1]						
	R1 /Ω	Q1 /μF	n_1	R2 /kΩ	Q2 /μF	n_2	k_{et} / s^{-1}
Au-Cys-FMCA	49.50 (0.72)	2.20(3.57)	0.97 (0.44)	11.56 (27.61)	3.66 (1.59)	0.56 (1.09)	11.80
Au-Cys-FDCA	40.20 (0.66)	5.07 (1.08)	0.93 (0.18)	76.31 (6.20)	8.38 (2.40)	0.66 (3.46)	0.78
Au-Cys-SWCNT/FMCA	41.50(1.50)	8.00(1.86)	0.92 (0.36)	116.2(6.36)	16.19 (5.23)	0.77 (2.76)	0.27
Au-Cys-SWCNT/FDCA	18.90 (1.16)	4.32 (2.81)	0.94 (0..71)	24.16 (29.22)	2.16 (5.02)	0.66 (1.27)	9.56

[1].The value in brackets are the estimated error percentages.

Thus, the n_1 values in Table 5.2 are approximately close to 1.0 for an ideal capacitive behaviour, while the n_2 (that replaced the Warburg diffusion) are in the range between 0.56 and 0.77, describing the porous nature of the adsorbed film on the gold electrode.

The phase angles seen on the Bode plots (i.e., –phase angle (ϕ) vs log f, Figure 5.4(a)) are in the range of 75 - 80°, which are less than the 90° expected of an ideal capacitive behaviour. Figure 5.4(b) illustrates the relationship between the logarithm of impedance and frequency. The slopes of the Bode plots (log Z vs log f) are approximately similar (*ca*. –0.82, r^2 = 0.992) at the mid frequency region, indicative of pseudocapacitive behaviour. At high frequency regions, the slopes are almost zero, indicative of resistive behaviour at these high frequency regions.

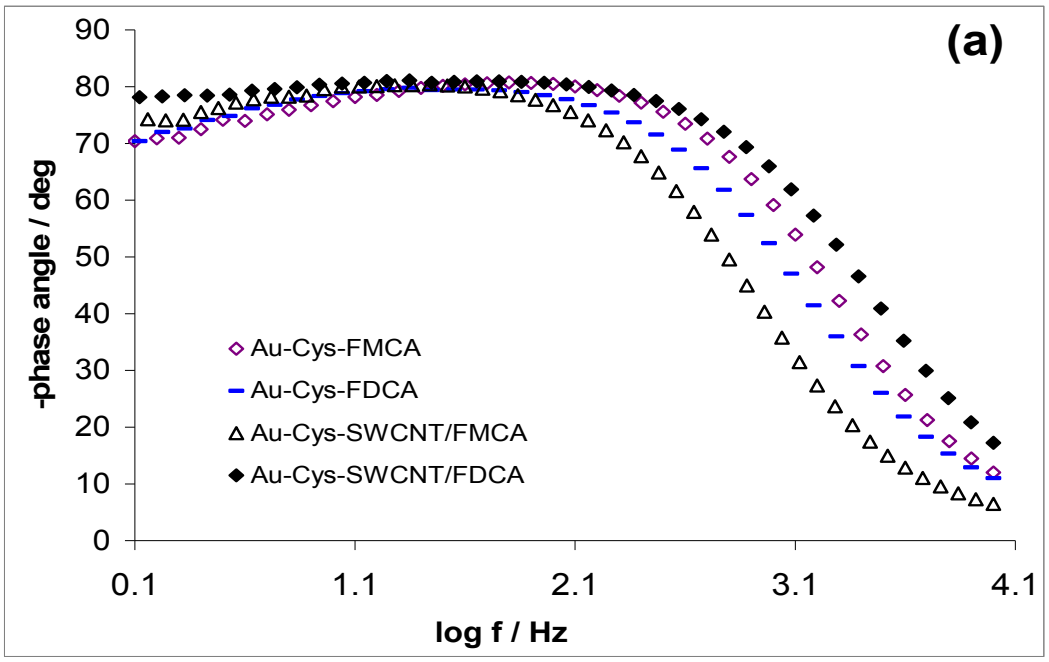

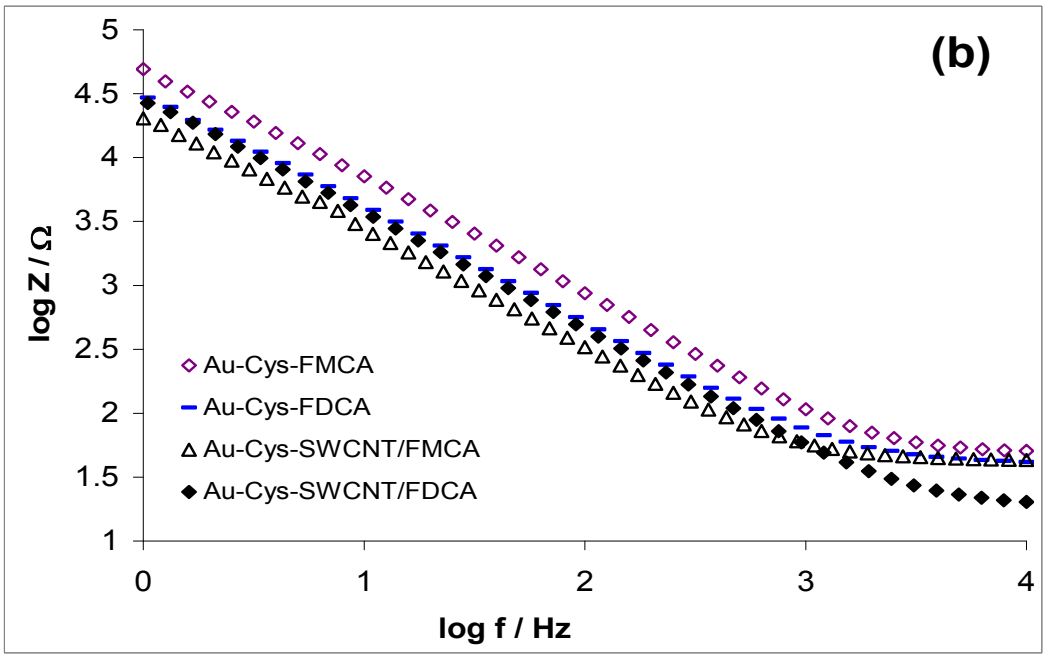

Figure 5.5: Bode plots, phase angle vs log f (a) and log Z vs log f (b),of the logarithm impedance spectra versus frequency of the modified electrodes in 0.5M H_2SO_4.

5.4 Electron transfer dynamics in a redox probe, $[Fe(CN)_6]^{4-}$ / $[Fe(CN)_6]^{3-}$

5.4.1 Cyclic voltammetric characterization

Electron transport properties of the electrodes were studied in PBS solution containing the outer-sphere redox probe, $[Fe(CN)_6]^{4-}$/ $[Fe(CN)_6]^{3-}$ (pH 7.2).

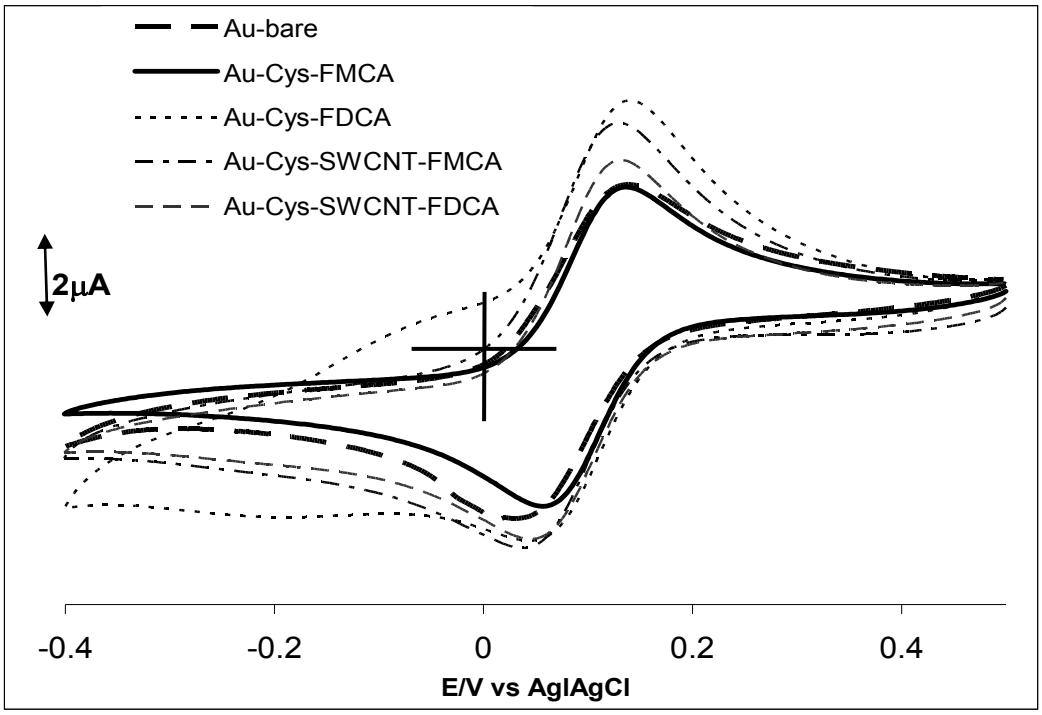

Figure 5.6: Comparative cyclic voltammetric evolutions of the bare and modified gold electrodes obtained in 0.1 M $[Fe(CN)_6]^{4-}$/$[Fe(CN)_6]^{3-}$ PBS, pH 7.2); bare Au, Au-Cys-FDCA, Au-Cys-FMCA, Au-Cys-SWCNT/FDCA and Au-Cys-SWCNT/FMCA. Scan rate = 25 mVs^{-1}.

Typical comparative cyclic voltammograms are exemplified in Figure 5.6. The ΔE_p value for all the electrodes are essentially the same (~ 110 mV) with same equilibrium potential ($E_{1/2} \approx 100$ mV).

5.4.2 Electrochemical impedimetric characterization

Since electrochemical impedance spectroscopy (EIS) provides a more detailed description of an electrochemical system [26] than cyclic voltammetry does, EIS was used to follow the electron transfer kinetics occurring at these electrodes. The EIS measurements were performed at the formal potential ($E_{1/2} \approx 100$ mV). Figure 5.7(a) shows examples of the Nyquist plots obtained for the electrodes in the $[Fe(CN)_6]^{4-}/[Fe(CN)_6]^{3-}$ solution (pH 7.2). The symbols in figure 5.7(a) represent the experimental data, while solid lines are the fitted curves fitted with the modified Randles equivalent circuit model (Figure 5.7(b)).

The EIS data together with the relative % errors is tabulated in Table 5.3 wherein the true capacitance is replaced by the constant phase element (CPE). In this model the R_s is the solution/electrolyte resistance, R_{ct} represents the electron-transfer resistance, while the Z_w is the Warburg impedance.

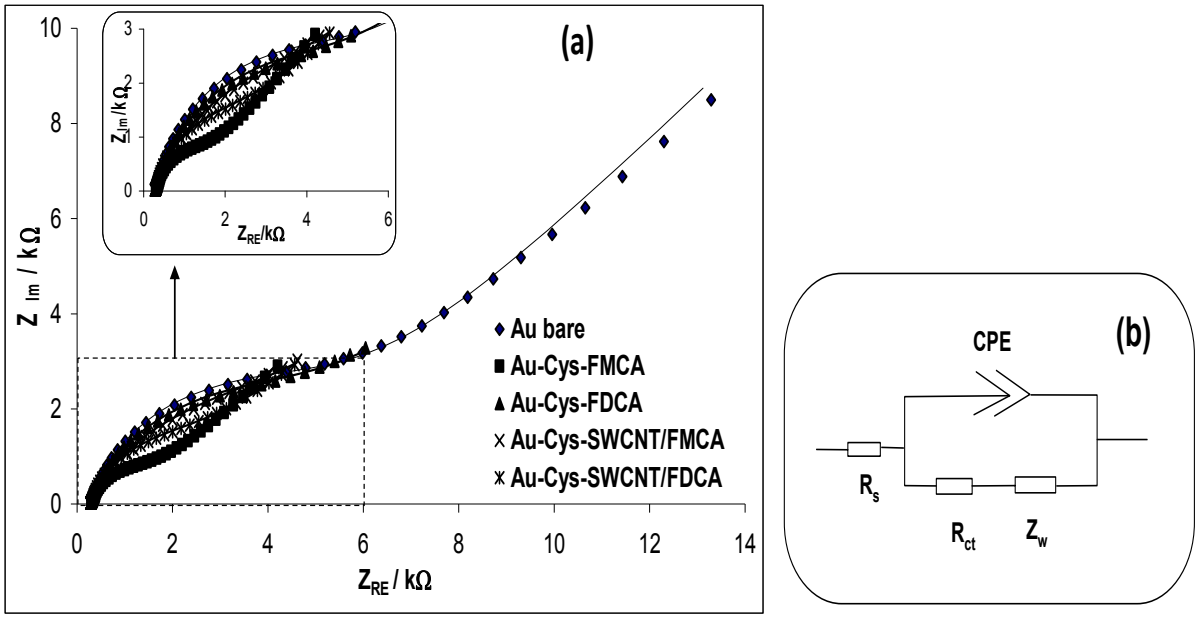

Figure 5.7: Nyquist plot (a) and the electrical equivalent circuit (b) used to fit the impedance spectra of bare Au and the modified electrodes obtained in 0.1 M $[Fe(CN)_6]^{4-}$/ $[Fe(CN)_6]^{3-}$ (PBS, pH 7.2).

The apparent electron transfer rate constant (k_{app}) of each of the electrodes was obtained from:

$$\mathbf{k}_{app} = \frac{RT}{n^2F^2AR_{ct}C} \qquad (5.4)$$

where n is the number of electron transfered (n=1), F is the Faraday constant, R is the ideal gas constant, T is the Kelvin temperature, A is the experimentally-determined area of the electrode, R_{ct} value is obtained from the fitted Nyquist plots, C is the concentration of the $[Fe(CN)_6]^{3-}$ (in mol cm^{-3}, the concentration of $[Fe(CN)_6]^{3-}$ and $[Fe(CN)_6]^{4-}$ are equal).

Table 5.3: Summary of estimated EIS parameters obtained in 0.1 M $[Fe(CN)_6]^{4-}$/ $[Fe(CN)_6]^{3-}$ (PBS, pH 7.0)

	Electrochemical impedance spectroscopic parameters[a]					
Electrodes	R_s /Ω	CPE /μF	n	Rct /kΩ	Z_W /μΩ	10^3 k_{app}/cm s^{-1}
Au	305.8(0.43)	5.32(2.02)	0.86(0.37)	5.12(1.15)	104.0(0.90)	1.93±0.02
Au-Cys-FMCA	300.9(0.40)	0.44(4.16)	0.86(0.58)	1.41(1.64)	98.3(0.68)	6.98±0.11
Au-Cys-FDCA	310.0(0.63)	0.63(5.56)	0.82(0.69)	4.93(3.03)	118.7(4.52)	2.00±0.06
Au-Cys-SWCNT/FMCA	271.7(0.53)	0.52(5.59)	0.76(0.68)	4.65(3.87)	126.6(4.67)	2.12±0.08
Au-Cys-SWCNT/FDCA	280.1(0.33)	0.98(3.22)	0.86(0.45)	2.58(1.83)	107.6(1.28)	3.82±0.07

[a] The value in brackets are the estimated error percentages.

From Table 5.3, the k_{app} values increases as follows: Au-Cys-FMCA > Au-Cys-SWCNT/FDCA > Au-Cys-SWCNT/FMCA ≈ Au-Cys-FDCA > bare Au. Within the limits of experimental errors, the trend in the electron transport kinetics seen in the redox probe ($[Fe(CN)_6]^{3-}$ /$[Fe(CN)_6]^{4-}$ solution are somewhat comparable with those observed with the H_2SO_4 solution. However, we should not expect them to necessarily follow the same trend. This is because, first, the experiments were performed at different electrolyte conditions. Second, unlike the experiment in the H_2SO_4 that provides insight into the redox processes (Fe^{3+}/Fe^{2+}) of the electrode-confined ferrocene species, the experiment with the $[Fe(CN)_6]^{3-}/[Fe(CN)_6]^{4-}$ solution essentially interrogates the extent to which the immobilized ferrocene species permit the permeation of the redox probe and/or enhance faradaic response of the $[Fe(CN)_6]^{3-}$ and $[Fe(CN)_6]^{4-}$ species. The *n* values (Table 5.3) are in the range 0.76 and 0.86, indicative of pseudocapacitive behaviour. The values of the phase angles of less than 90^o confirm the pseudocapacitive behaviour as well as the slopes of the log *Z* vs log *f* plot (*ca*. –0.57) as illustrated in figures 5.8(a) and 5.8(b), respectively. Figure 5.8(b) also illustrates high frequency which approximate high rate of reaction, thus this bode plot agrees with Table 5.3.

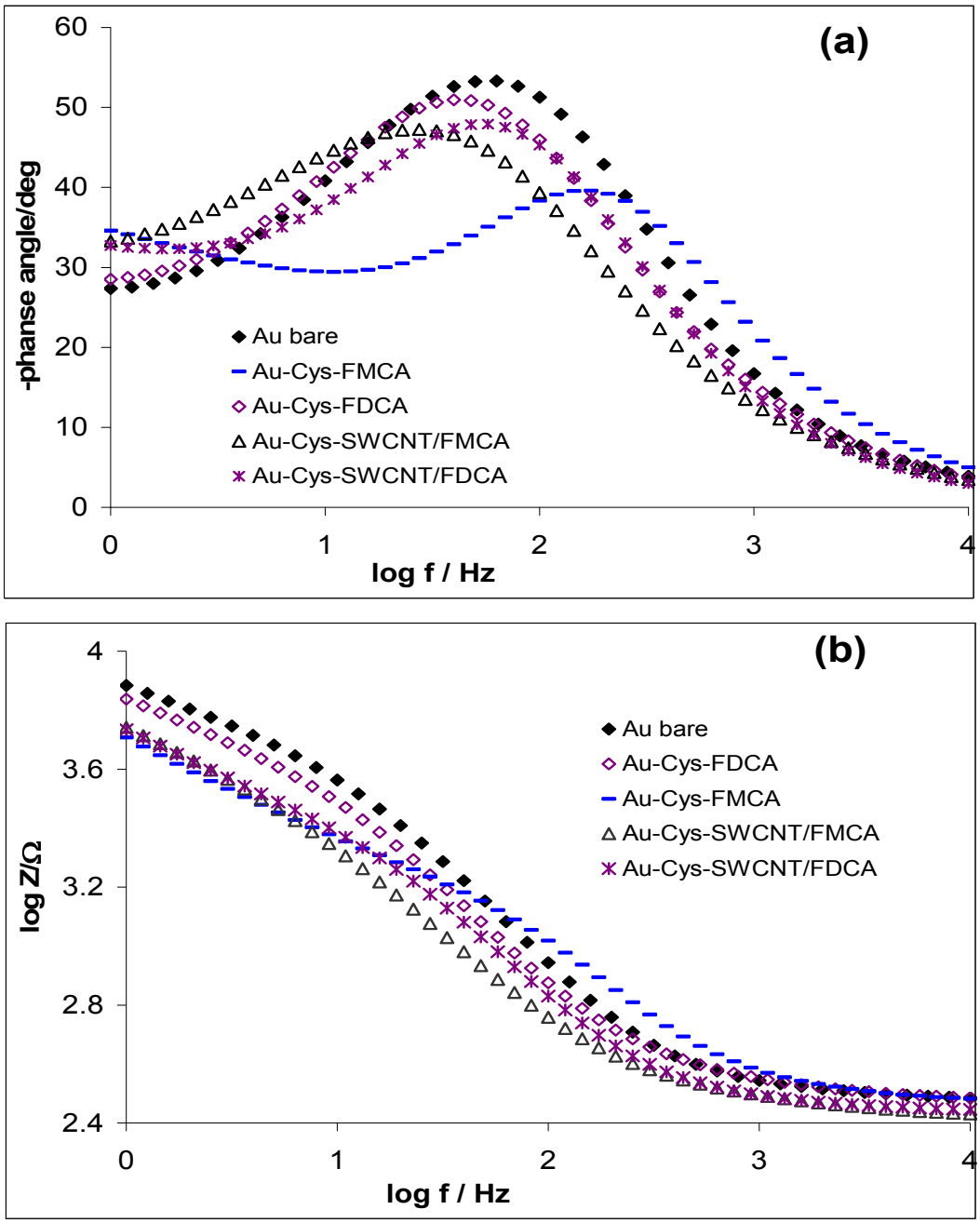

Figure 5.8: Bode plots, phase angle vs log f (a) and log Z vs log f (b) of the impedance spectra of the modified electrodes in redox probe ($[Fe(CN)_6]^{4-}/[Fe(CN)_6]^{3-}$) PBS solution (pH 7.2).

REFERENCES

1. J. Yu, J. G. Shapter, J. S. Quinton, M. R. Johnston and D. A. Beattie, Phys. Chem. Chem. Phys. 9 (2007) 510.
2. J. J. Gooding, R. Wibowo, J. Liu, W. Yang, D. Losic, S.Orbons, F.J. Meams, J.G. Shapter and D.B. Hibbert, *J. Am. Chem. Soc.*125 (2003) 9006.
3. J. J. Gooding, *Electrochim. Acta* 50 (2005) 3049.
4. J. J. Gooding, A. Chou, J. Liu, D. Losic, J. G. Shapter,; Hibbert, D. B. *Electrochem. Commun.* 9 (2007) 1677.
5. K. O. Ozoemena, T. Nyonkong *Electrochim. Acta* 47 (2002) 4035.
6. K. O. Ozoemena, T. Nyonkong, P. Westbroek, *Electroanalysis* 14 (2003) 1762.
7. H. O. Finklea, In: A. J. Bard, I. Rubinstein, (Eds.), *Electroanalytical Chemistry*, Marcel Dekker, New York, 19 (1996) 109.
8. H. O. Finklea, *J. Am. Chem. Soc.* 114 (1992) 3173.
9. H. O. Finklea, M. S. Ravenscroft, and D. A. Snider, *Langmuir* 9 (1993) 223.
10. B. S. Flavel, J. Yu, A. V. Ellis, J. G. Shapter, *Electrochim. Acta* 54 (2009) 3191.

11. G. K. Rowe, M. T. Carter, J. N. Richardson, and R. W. Murray, *Langmuir* 11 (1995) 1797.

12. S. Chen, R. W. Murray *J. Phys. Chem*. B 103 (1999) 9996.

13. S. Chen, *J. Phys. Chem. B*, 104 (2000) 663.

14. C. E. D. Chidsey, C. R. Bertozzi, T. M. Putvinski, A. M. Mujsce, *J. Am. Chem. Soc.* 112 (1990) 4301.

15. C. E. D. Chidsey, *Science* 251 (1991) 919.

16. R. W. Murray, In *Electroanalytical Chemistry*; Bard, A. J., Ed.; Marcel Dekker: New York, 13 (1984) 191.

17. R. C. Chambers, C. E. Inman, J. E. Hutchinson, *Langmuir* 21 (2005) 4615.

18. H. O. Finklea In *Electroanalytical Chemistry*; A. J. Bard, Ed.; Marcel Dekker: New York, Vol. 19 (1996) p 109.

19. S. E. Creager, T. T. Wooster, *Anal. Chem*. 70 (1998) 4257.

20. L. V. Protsailo, W. R. Fawcett, *Electrochim. Acta*. 45 (2000) 3497.

21. M. I. Prodromidis, *Electrochim. Acta*. doi:10.1016/j.electacta.2009.01.081 (2009).

22. N. S. Mathebula, J. Pillay, G. Toschi, J. A. Verschoor, K. I. Ozoemena, *Chem. Commun*. (2009)3345.

23. E. Barsoukov, J. R. Macdonald, *Impedance Spectroscopy: Theory Experiment, and Applications*; 2nd ed.; Wiley: Hoboken, New Jersey, 2005; chapters 1 – 4.

24. M. E. Orazem, B. Tribollet, *Electrochemical Impedance Spectroscopy*; John Wiley & Sons Inc: Hoboken, NJ. 2008; Chapter 13.

25. V. Ganesh, S.Pitchumani, V. Lakshminarayanan, *J. Power Sources* 158 (2006) 1523.

26. B. –Y. Chang, S. -Y.Hong, J. -S. Yoo and S. -M. Park, *J. Phys. Chem. B* 110 (2006) 19385.

CHAPTER 6

ELECTROCATALYTIC PROPERTIES OF FERROCENE SINGLE-WALLED CARBON NANOTUBES BASED ELECTRODES: THIOCYANATE AS A MODEL ANALYTE

6.1 Square wave voltammetric detection of SCN^-

Having established that the neighbouring SWCNTs impact on the electron transfer of the ferrocene molecular assemblies (chapter 5), it was necessary to establish the extent to which these SWCNTs could impact on the electrocatalytic behaviour of the ferrocenes. For this study, thiocyanate (SCN^-) was chosen as a model analyte. Figure 6.1 is a comparative square wave voltammetric (SWV) evolutions obtained at constant concentration (1 mM) of SCN^- at the various electrodes in PBS (pH 4.8). This pH condition was chosen for this experiment as it is well known for enhanced detection of SCN^- [1-2]. The catalytic behaviour (in terms of onset potential) follows this trend: Bare Au (0.64 V) > Au-Cys-SWCNT (0.62 V) > Au-Cys-FMCA ≈ Au-Cys-FDCA (0.48 V) > Au-Cys-SWCNT/FMCA (0.50 V) > Au-Cys-SWCNT/FDCA (0.42 V).

The Au-Cys-SWCNT/FDCA and Au-Cys-SWCNT/FMCA gave the highest current response with less positive onset potential (0.3 V) compared to other electrodes. However, Au-Cys-SWCNT/FDCA recorded the least peak potential for the oxidation of SCN^- at 0.48 V, possibly due to the repulsive interaction between the negatively charged SCN^- and high number of surface –COOH species at the FDCA.

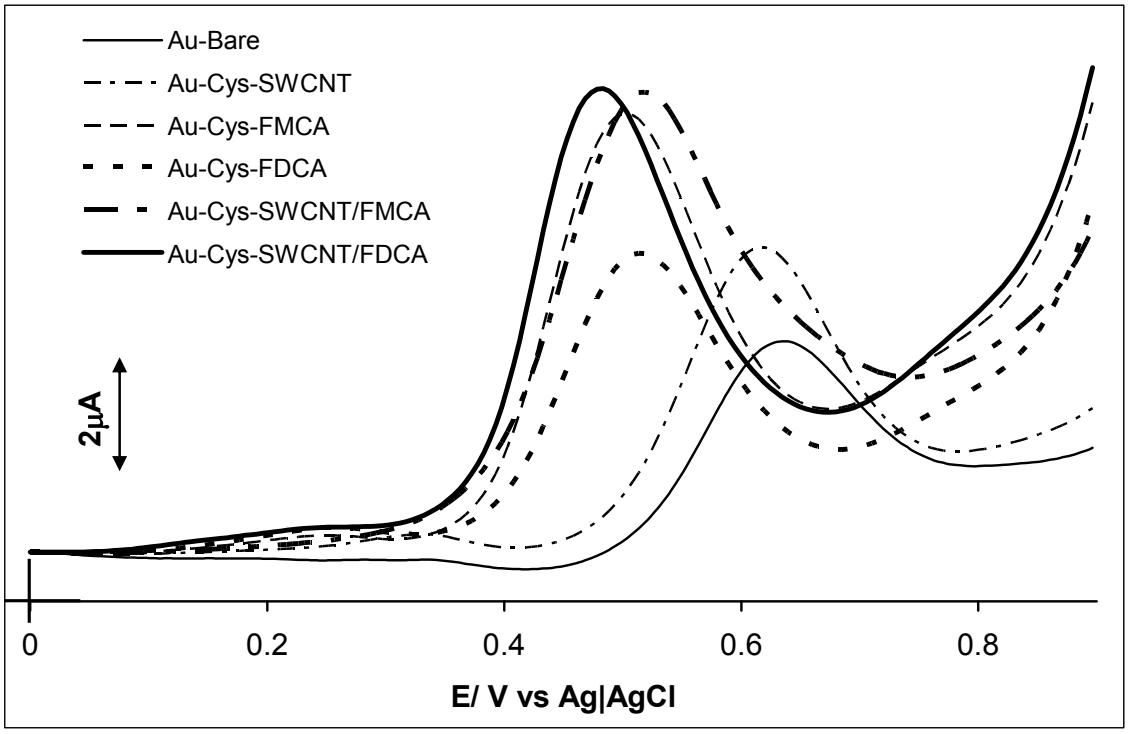

Figure 6.1: Comparative square wave voltammograms of the bare gold and modified gold electrodes obtained in PBS solution (pH 4.7) containing 1 mM SCN^-.

Second, the ferrocene-based electrode without the SWCNTs (i.e., Au-Cys-FDCA and Au-Cys-FMCA) exhibited more positive onset potential (~ 0.35 V) for the oxidation of SCN^- compared to the ones containing SWCNTs (Au-Cys-SWCNT/FDCA and Au-Cys-SWCNT/FMCA) at 0.3 V. This improved response towards the detection of SCN- species is due to the combined synergistic activities of good electrocatalysts (FCDA or FMCA) and the efficient electronic conducting nanowires (SWCNTs). This finding is quite remarkable especially when compared to data

previously obtained at the FePc and SWCNT-FeOHETPc SAM modified electrodes where the oxidation of SCN^- occurred at peak potentials ≥ 0.60 V [2]. Also, the current responses recorded in this present work for the Au-Cys-SWCNT/FDCA and Au-Cys-SWCNT/FMCA for the same concentration of SCN^- (1 mM) is approximately twice than reported for the FeOHETPc and FePc-SAM modified electrodes [2].

6.2 Influence of scan rates on electrocatalysis of SCN^-

Oxidation of SCN^- using cyclic voltammetric experiments were carried out with a view to establishing the impact of scan rates (ν) at constant concentration (1 mM) of the SCN^-. The study was carried out with Au-Cys-SWCNT/FDCA electrodes as illustrated in figure 6.2. The increase in the peak current was observed with increasing scan rates (scan rates ranging 25 - 900 mV/s). Also, a broad reduction peak (in the 0.1 to 0.5 V regions) appeared only at higher scan rates, > 100 mVs^{-1}. A similar behaviour of the electrode was observed for the electrode modified with FeOHETPc as discussed in chapter 4. The insert in figure 6.2 indicate a plot of I_p vs ν, which is not linear proving that neither the oxidized SCN^- nor its intermediate product(s) adsorbed on the modified electrode.

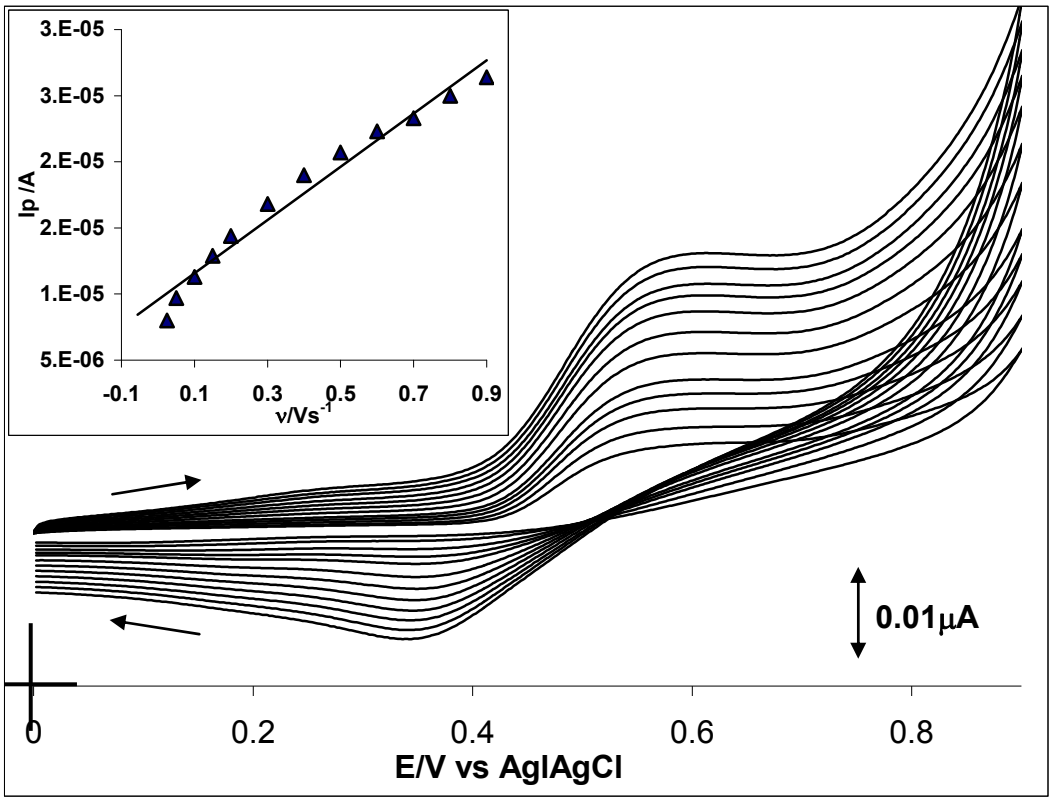

Figure 6.2: Cyclic voltammetric evolutions at varying scan rates and insert is the plot of current (I_p) versus scan rate (ν) ranging from 25 to 900 mVs^{-1}. [SCN^-] = 1 mM

Figure 6.3(a) illustrates the relationship between peak current (I_p) with the square root of scan rate ($\nu^{1/2}$) of the SCN^- oxidation which gave a linear relationship (R^2 = 0.9989), indicating a diffusion-controlled reaction. Tafel plot (see equation 4.1) is given in figure 6.3(b) where two slopes can be seen [3]. The first slope for lower potential, i.e between 555 and 578 mV vs AgIAgCl leads to a value of 30 mV / decade and the second slope for higher potential between 600

and 620 mV which lead to a value of 66 mV / decade. This is an indication of the two mechanisms that are involved as a function of potential for Au-Cys-SWCNT/FDCA electrode.

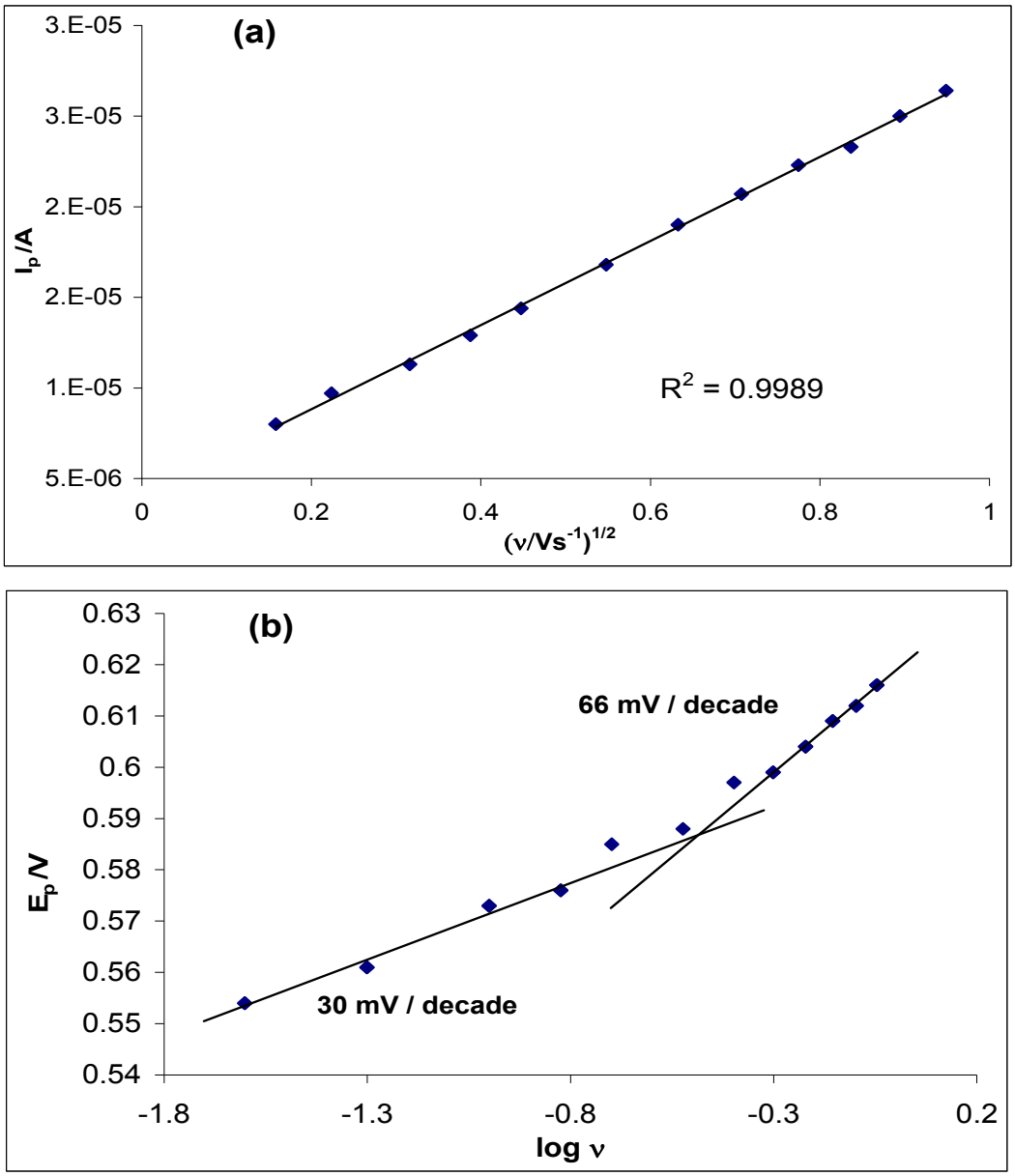

Figure 6.3: The plots of (a) peak current against the square root of the scan rate and (b) peak potential against log of scan rate for the Au-Cys-SWCNT/FDCA electrode in 1 mM SCN^-.

6.3 Rotating gold disk electrode experiments

The rotating disk electrode (RDE) voltammetric evolutions of constant concentration (1 mM SCN^-) at different rotating speed of the electrodes are shown in Figure 6.4. The Koutecky-Levich plot (Figure 6.4 inset) was obtained from the conventional Koutecky-Levich theory. The numbers 1 to 12 in the figure correspond to 250, 500, 750, 1000, 1250, 1500, 1750, 2000, 2250, 2500, 2750 and 3000 rpm, respectively.

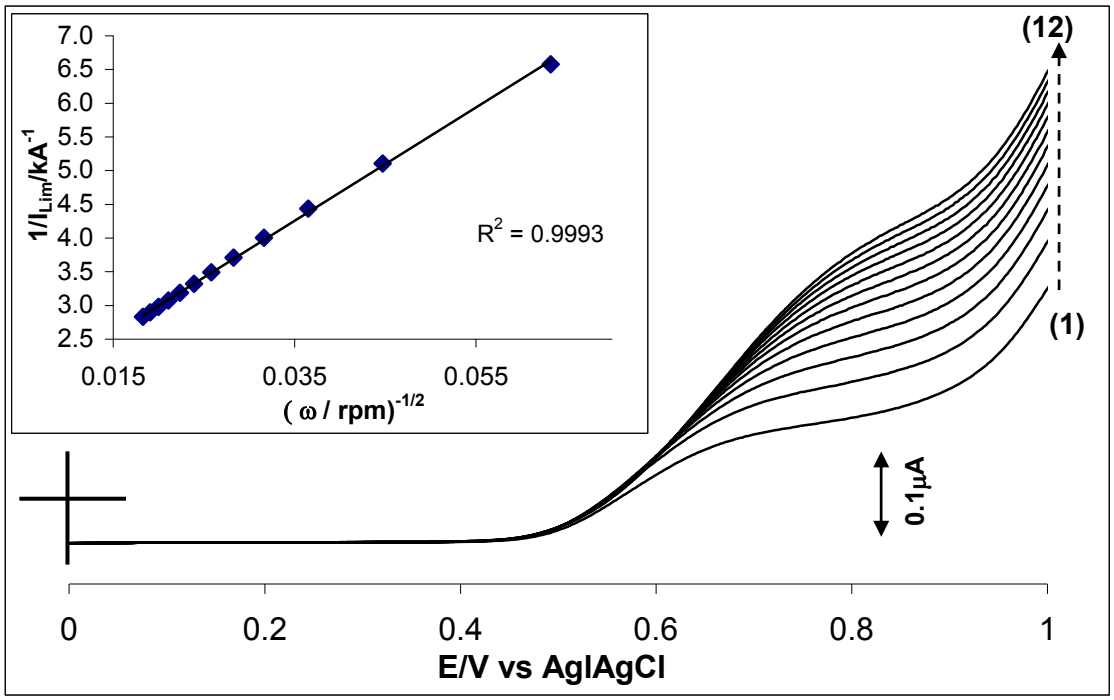

Figure 6.4: Linear sweep voltammetric evolutic evolutions of the rotating disk electrode experiments obtained at Au-Cys-SWCNT/FDCA in PBS solution (pH 4.8) containing 1 mM SCN^- at 50 mVs^{-1}. (Inset is Koutecky-Levich plot).

The results showed that the catalytic current increased linearly with increasing $\omega^{-1/2}$ with a positive intercept, indicating that the electrode reactions were controlled by both kinetics and the mass transport of SCN^- species at the electrode surfaces. From the intercept and the slope of the plot, the diffusion coefficient value of *ca*.1.10 x 10^{-5} cm^2s^{-1} was obtained. This value is of same magnitude as the phthalocyanine based electrode (chapter 4) with similar experimental conditions. The surface coverage of the Au-Cys-SWCNT/FDCA electrode was calculated as 1.4 x 10^{-9} mol cm^{-2} (see table 4.1). This value suggests that the material on the gold electrode is not a monolayer which confirms the conclusion made in chapter 4 that it is possible that the high surface coverages obtained in our experiments could be due to the long exposure time of cysteamine to gold electrode leading to more binding sites for the ferrocenes. Using the Koutečky-Levich equation, the k value was obtained *ca*. 2.0 x 10^{-2} cm^3 mol s^{-1}.

6.4 Chronoamperometric investigations

A well resolved double-step chronoamperometric evolutions obtained at the Au-Cys-SWCNT/FDCA electrode in the absence (buffer alone) and presence of consecutive addition of 32.3 μM thiocyanate in phosphate buffer solution (pH 4.8) is shown in figure 6.5. The figure illustrates the double potential step chronoamperometric experiments recorded by polarizing the working electrode potentials to 0.62 and 0.20 V. It shows that at the conditions employed for this work, the SCN^- was irreversible. Figure 6.5 (inset) depicts linearity with slope of 7474.3 between I_p versus [SCN^-]. The linear concentration range of up to 0.21 mM was obtained for the Au-Cys-SWCT/FDCA electrode with a sensitivity of ca. $7.5x10^{-3}$ AM^{-1}, and limit of detection ~ 28 μM (LoD = 3.3 s/m [4], where s is the relative standard deviation of the intercept and m the slope of the linear peak current vs the concentration of SCN^-). The Cottrell equation (Equation 6.1) was used to determine both diffusion coefficient (D) and catalytic rate constant of SCN^- from the chronoamperometric data.

$$I = \frac{nFAD^{1/2}C}{\pi^{1/2}t^{1/2}} \qquad (6.1)$$

where n = number of electrons involved in the reaction, F is the Faraday constant F (96485 C mol^{-1}), and A is the experimentally

determined area of the electrode, C is the bulk concentration of the thiocyanate (mol/L)), while t is time (s).

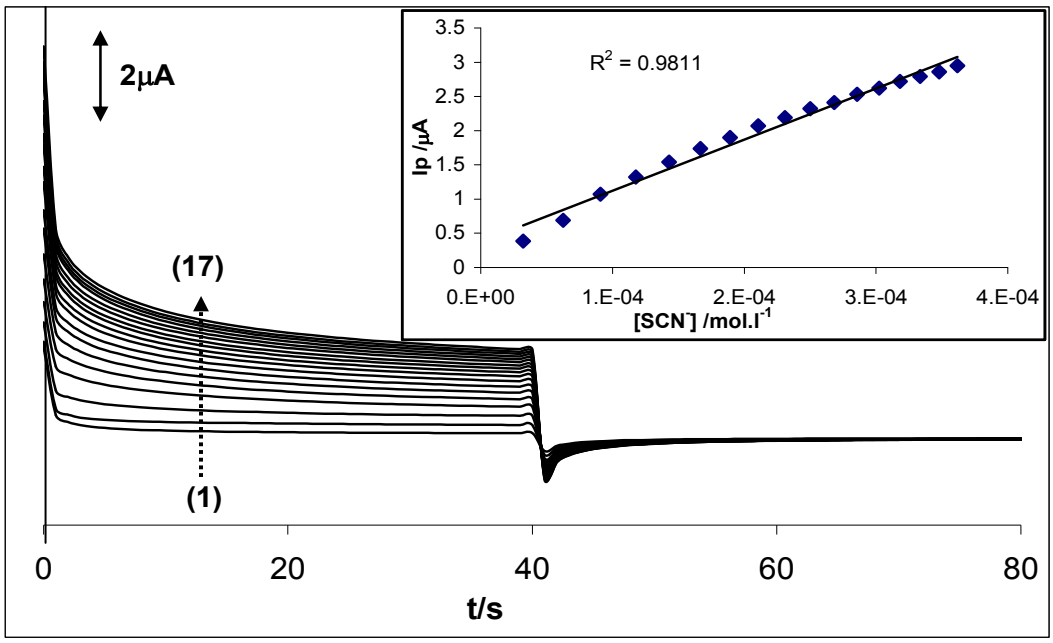

Figure 6.5: Typical double potential step chronoamperometric transients at Au-Cys-SWCNT/FDCA in PBS solution (pH 4.8) following addition of SCN^- Inset is the plot of chronoamperometric current at t = 10 sec vs [SCN^-].

Figure 6.6 shows the linear plots of I_p *vs* $t^{-1/2}$ at different thiocyanate concentrations, and from the plot of slopes vs [SCN^-], and taking n = 2, the D value for SCN^- was estimated to be *ca.* 10.4 x 10^{-10} cm^2s^{-1}, which is lower than that obtained for the FeOHETPc based electrode (~ 10^{-6} cm^2s^{-1}). Despite this low D value, the catalytic properties of ferrocene based electrode is still more enhanced than

that of the FePc. The catalytic rate constant for the oxidation of SCN^- was also estimated from the chronoamperometry experiments using the relationship [5,6] (Equation 6.2):

$$\frac{I_{cat}}{I_{buff}} = \pi^{1/2}(kCt)^{1/2} \qquad (6.2)$$

where I_{cat} and I_{buff} are the currents in the presence and absence of thiocyanate, respectively; k is the catalytic rate constant and t is the time in seconds. From the plots of I_{cat}/I_{buff} vs $t^{1/2}$ at different thiocyanate concentrations (Figure 6.7), and a plot of the slopes vs $[SCN^-]$, k was estimated as 1.26×10^4 cm^3 mol s^{-1}.

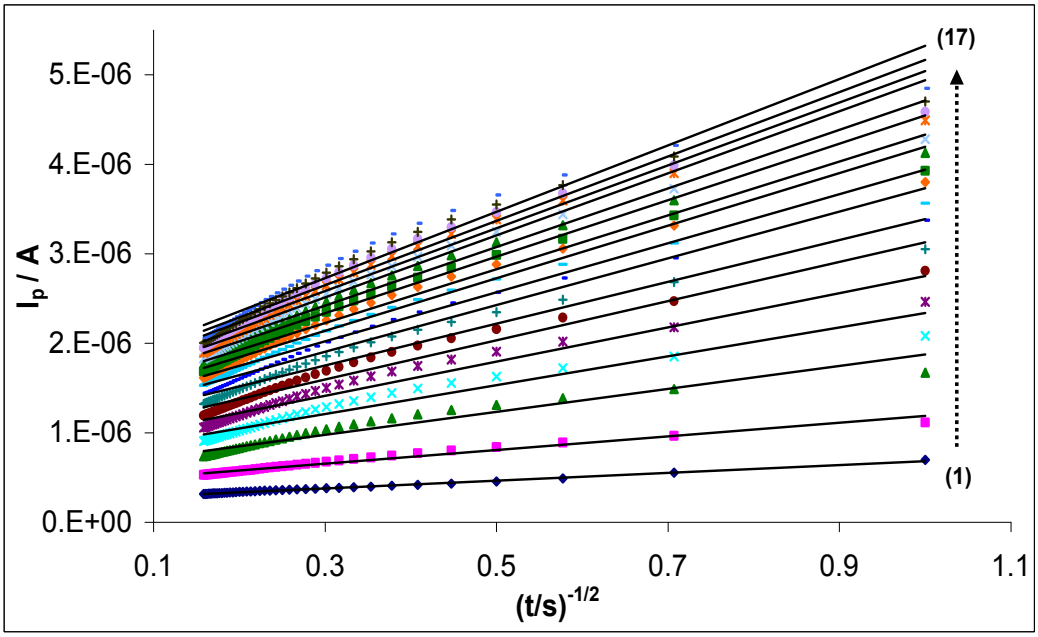

Figure 6.6: Typical Cottrell equation plots obtained from the chronoamperometric evolution at Au-Cys-SWCNT/FDCA in PBS solution (pH 4.7) following addition of SCN^-.

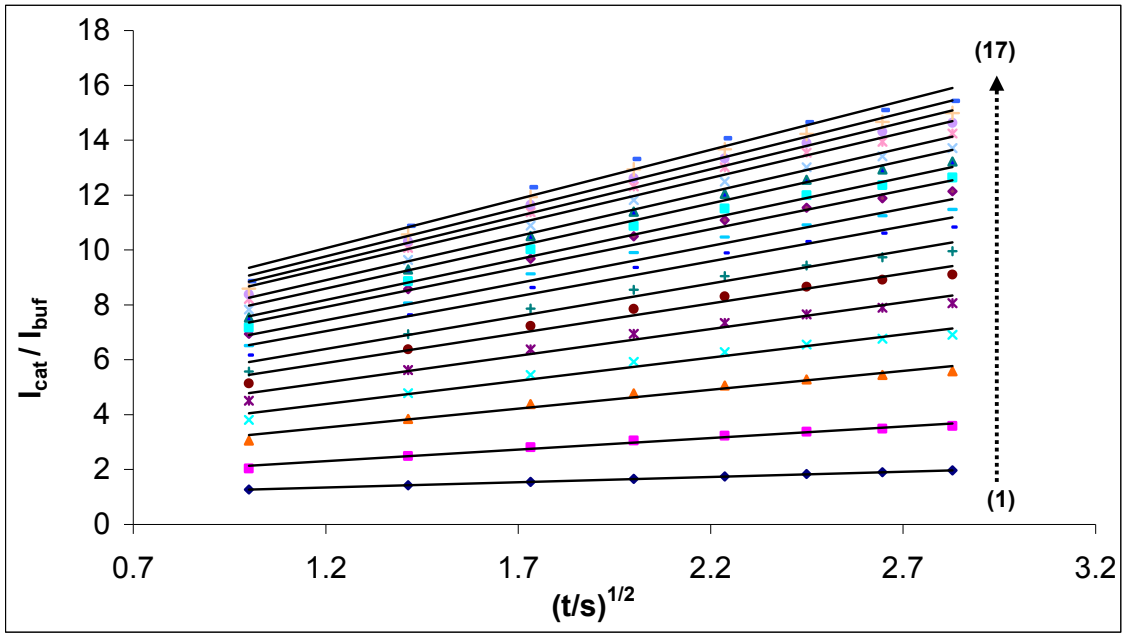

Figure 6.7: Plots of I_{cat}/I_{buff} vs $t^{1/2}$ obtained from the chronoamperometric evolution at Au-Cys-SWCNT/FDCA in PBS solution (pH 4.7) following addition of SCN^-.

6.5 Gold nanoparticle-modified indium tin oxide electrode experiment

The suitability of the ITO-nanoAu-Cys-SWCNT/FDCA for a possible application as a disposable, one-shot electrode system for a quick chronoamperometric detection of SCN^- was also tested (Figure 6.8). With this electrode, a chronoamperometric sensitivity of 7.3 $x10^{-3}$ and a limit of detection of ~13 nM for the SCN^{-1} were obtained. The values are comparable to the data obtained at the modified bulk gold electrode.

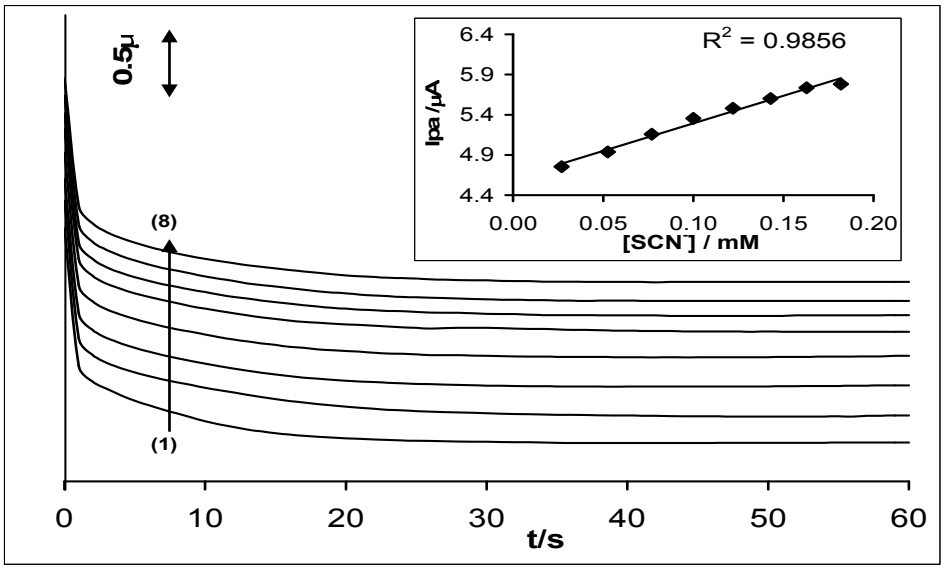

Figure 6.8: Chronoamperometric evolutions at ITO-nanoAu-Cys-SWCNT/FDCA electrode in PBS solution pH 4.7 containing 1mM SCN^-. **inset**: Plot of peak current vs concentration obtained from chronoamperometric evolutions for the ITO-nanoAu-Cys-SWCNT/FDCA electrode.

REFERENCES

1. S. Adak, A. Mazumdar, R. K.Banerjee, *J. Biol. Chem.* 272 (1997) 11049.
2. K. I. Ozoemena, T. Nyokong, *J. Electroanal. Chem.* 579 (2005) 283.
3. S. Baranton, C. Coutanceau, E. Garnier and J. –M. Leger, *J. Electroanal. Chem.* 590 (2006) 100.
4. G. D. Christian, Analytical Chemistry, 6th ed. John Wiley and Sons, New York, 2004, p.113.
5. M. H. Pournaghi-Azar, R. Sabzi, *J. Electroanal. Chem.* 543(2003) 115.
6. K. M. Manesh, P. Santosh, A. I. Gopalan, K. -P. Lee, *Electroanalysis* 18 (2006) 894.